geosciences

MDPI

Article

The Influence of the DSM Spatial Resolution in Rockfall Simulation and Validation with In Situ Data

Maria P. Kakavas, Konstantinos G. Nikolakopoulos *, Aggeliki Kyriou and Ioannis Koukouvelas

Division of Applied Geology and Geophysics, Department of Geology, University of Patras, 26504 Patras, Greece
* Correspondence: knikolakop@upatras.gr; Tel.: +30-2610997945

Abstract: Remote sensing constitutes an advantageous tool towards the landslide/rockfall susceptibility mapping by incorporating optical satellite or radar data and photogrammetric data in Geographical Information System environment. A plethora of rockfall data can be derived by gigital surface models (DSMs). This article focuses on the effect of the spatial resolution of DSMs in rockfall investigations solely. DSMs with pixel size ranging from 5 cm to 90 m were taken into account for the study of three different rockfall events occurring in Western Greece, namely, at Moira, Myloi and Platiana settlements. Elevation profiles along the rockfall bodies were created from the diverse DSMs in GIS environment. Then, these profiles were implemented into the RocFall software for 2D rockfall simulations. The produced simulations were evaluated against their spatial resolution of DSMs and were confirmed with field observations and measurements. The ultimate scope of this paper is to conclude to the most appropriate DSM for rockfall simulations via RocFall software. It is observed that DSMs with high spatial resolution depicted a detailed and realistic topography, while DSMs with coarse/low resolution flattened the surface roughness. As rockfall simulations are linked to slope profile, this observation has an impact on RocFall outcomes. According to this study the most appropriate DSM, pertaining to this type of research, is the UAV, which produces the more accurate and realistic results. These results were assessed through the use of in situ measurements taken by the real rockfall events.

Keywords: rockfalls; rockfall software; DSMs; spatial resolution; slope profiles

Citation: Kakavas, M.P.; Nikolakopoulos, K.G.; Kyriou, A.; Koukouvelas, I. The Influence of the DSM Spatial Resolution in Rockfall Simulation and Validation with In Situ Data. *Geosciences* **2023**, *13*, 57. https://doi.org/10.3390/geosciences13020057

Academic Editors: Jesus Martinez-Frias and Laura Longoni

Received: 5 January 2023
Revised: 30 January 2023
Accepted: 9 February 2023
Published: 14 February 2023

1. Introduction

Rockfall activity is a physical phenomenon linked either to endogenous factors, such as earthquakes and volcanic activities, or to exogenous factors, such as heavy rainfalls, avalanches, anthropogenic processes, etc. Moreover, rockfall triggering factors can be distinguished between natural (e.g., rainfall, weathering, freeze–thaw, root wedging, snow melt, wind, erosion, earthquake and volcano activity) [1–3] or anthropogenic (e.g., explosions, vibrations, deforestation, etc.) [4]. In addition, many rockfall phenomena are linked to karst processes, as karst environments are extremely susceptible to rock failures [5–7]. Rockfall catastrophes and fatalities motivated many researchers to focus on mapping slope instabilities, aiming to predict and minimize the negative effects of a failure event. The instability or stability of slopes can be measured through rockfall hazard assessment, appraisal of hazard, hazard zoning, risk analysis and susceptibility mapping methods. The increased demand in rockfall investigation leads to the production of various software for rockfall two-dimensional (2D) or three-dimensional (3D) simulation. Each software has different characteristics, input parameters and extracted data. For example, the 2D software, RocFall, requires parameters such as surface roughness, slope geometry and coefficient of restitution, while the 3D software STONE requires a digital terrain model (DTM), representing topography in raster format [8]. In general, parameters related to slope characteristics are used. The most common extracted data measurements pertain to the kinetic energy, the highest distance and the bouncing point. Three-dimensional simulation

methods usually give more reliable results, as more topographic parameters are taken into account. Consequently, the topographic illustration is closer to the real one. The choice of the most appropriate method for research depends on the extent of the rockfall event, the existing surface roughness data, the access to the in situ observation and the availability of time for analysis.

The most widely used 2D rockfall software is RocFall, as a plethora of slope materials are well calibrated in it [8,9]. Probabilistic analysis, rockfall prediction and remedial actions–measures design are all functions of this tool [10]. RocFall requires some crucial parameters to achieve landslide simulations and block trajectory depictions such as surface roughness, slope geometry and coefficient of restitution [11,12]. Reliable risk analysis by rating slope stabilities and slope mass classifications [13] as well as delineation of unstable areas and suggestions of possible remedial measures can be reached with the use of the software [14]. In addition, investigation of slope condition is in connection with the performance of kinetic energy and rockfall simulations. Thus, their determination leads to vulnerable areas zoning via RockFall [15,16]. The type of the geological material, such as slopes from various lithological blocks, affects the rockfall path [17]. Geological discontinuities and the size of dislodged blocks should be determined for the production of landslide distribution maps for every single slope profile [18,19]. The mass of falling block is proportional to the kinetic energy [20] and, also, the kinetic energy augments with rocks of higher mass [21].

The comparison of rockfall data and the selection of the most trustworthy results have led many researchers to the use more than one method or software [22–25]. Finite element program RS2™ for analyzing failure progression, RocFall for landslide assessment of rock slope profiles and Dan-W™ software for runout assessment of failure zones are methods for modeling rockfall investigation [26]. V-shaped gully (V-gully) method designs control effects through rainfall discharge and kinetic energy reduction, MSARMA software determines surface sliding positions and RocFall calculates slope movements from various slope angles. These three methods provide up-to-date rockfall prevention techniques [27]. Discrete element method achieves a landslide simulation closer to the real event, a detailed calculation process and a complete motion process, while RocFall software is simpler and depicts a broader area of rock block dispersion than the one observed in situ [28]. RocFall and CRSP [29] are both able to define the ideal slope geometry for the least rollout risk of falling blocks but the first provide more detailed results than the second [22]. In the lower parts of slope profiles, the results from CRSP and STONE exhibit high similarity, while, in the middle and upper slope parts, have the same velocity and heights to the ground from RocFall and STONE [23].

Digital surface models (DSMs) contribute to rockslide modeling either directly in a rockfall software (e.g., STONE) or indirectly (e.g., RocFall) through the use of slope profiles. The spatial resolution of DSMs affects rockfall simulation, as higher pixel sizes produce enhanced bounce heights and kinetic energies in both RAMMS (3D) and RocFall (2D) programs [24]. The use of a 2 m resolution digital terrain model (DTM) illustrates better an actual rockfall trajectory in Rockyfor3D, which is a 3D software, than in RocFall, which is 2D [25]. In many landslide investigations and existing rockslide simulation models, DSMs with high resolution and accuracy derived from LIDAR techniques were preferred for evaluating and characterizing rockfall trajectories [30], as these DSMs enable useful parameters to be gained, such as slope, curvature, aspect, flow direction, etc. [31]. DSM created by Greek National Cadastral and Mapping Agency have been also used for the selection of slope profiles. The high spatial resolution of this DSM (5 m) depicted a detailed 2D rockfall simulation via RocFall software [32]. The selection of SRTM30 DEM for slope profile extraction and aspect map production, in the same software, is more appropriate for large-scale events but without excluding smaller occurrences [33]. DSMs with cell sizes ranging from 1 m to 25 m have been tested though rockfall hazard investigation and high-resolution DSMs delineated accurate slope angles and profiles which are in accordance with the real topography.

The advantage of DSM use in rockfall mapping is the detection of rockfall sources in inaccessible steep slopes. The spatial resolution of DSMs affects the rockfall simulation procedure. The aim of this study is the determination of the degree of cell size influence in exported rockfall data from RocFall software. The aforementioned software processes slope profiles derived from DSMs; consequently, this is in conjunction with DSMs' accuracy. To this end, three different areas of interest, Moira, Myloi and Platiana settlement located in Peloponnese, in Western Greece were studied. In these settlements, recent events of rockfalls occurred between 2017 and 2019, causing huge disturbance in villager's lives. The under-study rockfall events are attributed to climatic phenomena without being triggered by strong ground motions during earthquakes. Intense rain precipitation, along with the corroded soil of those regions, lead to rockfall phenomena. In situ measurement and field observations took place and the collected data were compared with the software outputs. End-point rock locations, bounce heights and total kinetic energies were calculated via RocFall. Three slope profiles for each area were extracted from eight different DSMs, ranging from 5 cm to 90 m (Table 1), and were used by the software. The accuracy of the results was checked and was evaluated in accordance with the field measurements.

Table 1. Digital surface models used in the current study.

Dataset	Spatial Resolution (m)	Date of Data Acquisition	Date of DSM Release	Abbreviation for the Text
UAV DSM	0.05	After the rockfall occurrence	After the rockfall occurrence	UAV DSM
Cadastral DSM	5	2007–2008	2008	Cadastral
DSM from the Ministry of Agriculture	20	1995–1996	1996	AGRIC
ALOS AW3D30	30	2006–2011	2016	ALOS
SRTM30 DEM	30	2000	2015	SRTM30
ASTERGDEM	30	1999–2007	2009	ASTER
SRTM90 DEM	90	2000	2003	SRTM90
TANDEM-X	90	2010–2015	2016	TANDEM-X

2. Study Areas

2.1. Moira Settlement

Moira is a village located in Achaia prefecture of Peloponnese in northwestern Greece (Figure 1). The Alpine orogeny and post-Alpine period are the two main deformation periods for the NW part of Peloponnese so far. A high number of seismically active faults are linked with the post-Alpine deformation. The trend of these faults is WNW—or ENE [34,35]. Geodynamically active grabens and faults are closely related to rockslide events [36]. A series of factors such as extreme meteorological conditions (heavy rainfalls), deformation and extensively sheared lithologies lead to rockfall records of the wider area of Western Greece [37]. According to the geotectonic map of Greece, the broader area of interest belongs to Gavrovo and Pindos Units. Further, based on the geologic map of Greece, the above area consists primarily of Upper Cretaceous limestones (Hellenic Survey of Geology & Mineral Exploration—HSGME).

In particular, Moira village is located at the foot of Panachaiko–Erymanthos mountain and is close to the East Glafkos riverbank. Limestones with sparse vegetation, flysch deposits and siliceous and siliciclastic rocks are the predominant formations of the area. These formations have been affected by an imbricate system of thrust faults, with angles ranging from moderate to high, which consequently caused two rockfalls [38]. The first was in 19 January 2017 at 800 m elevation on an SE-facing slope of Panachaiko Mountain and the second was in 20 January 2017, which essentially was the main event. At the northwestern part of the area, where the rockfall occurred, a downslope movement of a huge volume of soil and rock was recorded. Subsequently, only a few minutes later from

the first record, at the southern part of the rockslide, a substantially higher volume of coarse debris slid and altered the slope profile. The volume of rock fragments displaced in Moira rockfall, on the road area and at the end of the slope profile, was estimated at 80 m^3 approximately. The lithological characteristics of the two parts were different. In the northwestern part, siliciclastic and/or siliceous lithologies were slid, while the southern part included limestones.

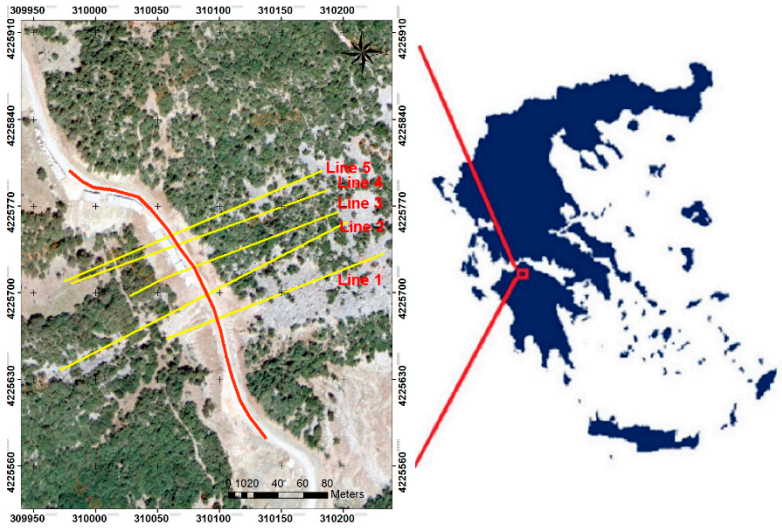

Figure 1. Slope profiles used in RocFall analysis regarding Moira region. The slope picture is taken from Greek Cadastral (2008).

In Moira rockfall five slope profiles were selected, aiming to achieve a 2D rockfall simulation via RocFall software (Figure 1). These profiles were extracted from seven different DSMs in ArcGIS environment: one 5 cm spatial resolution DSM created by UAV data, one 5 m DSM from the Greek Cadastral, three 30 m resolution DEMs (ALOS AW3D30 DEM, ASTER GDEM, and SRTM30 DEM) and two 90 m cell size DEMs (SRTM90 DEM and TanDEM_X). Subsequently, the geological and material characteristics of these slope profiles were defined (Table 2). The values of these characteristics were derived from in situ observations and published studies (Figures 2 and 3) [38,39]. In order to offer more realistic results, a barrier was considered at a certain point of the examined slope. In particular, this barrier is a local road which connects Moira with other villages. After the rockfall events, the road was covered with debris and restoring procedures were required.

Table 2. Geological and material characteristics.

MOIRA ROCKFALL	
Geological formation	Limestone with sparse vegetation
Date of the rockfall	20 January 2017
Length (m)	260
Width (m)	110
Slope profiles	3
Number of throw rocks	50
Barrier	1 road
Coefficient of normal restitution (Rt)	Mean: 0.47/St. dev. 0.04
Coefficient of tangential restitution (Rn)	Mean: 0.85/St. dev. 0.04
Friction angle (Phi)	Mean: 10/St. dev. 2
Horizontal velocity (m/s)	Mean: 22/St. dev. 2.2

Figure 2. Pictures taken from Moira region after rockfall event.

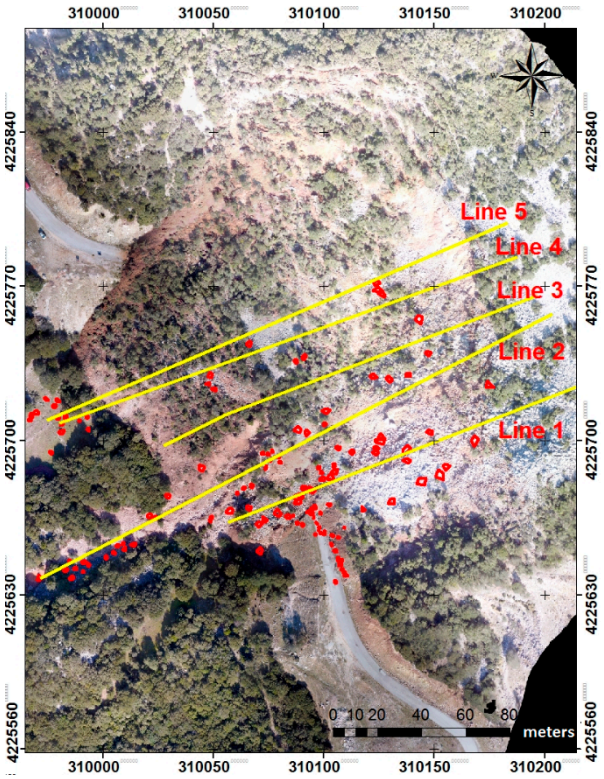

Figure 3. Picture of the rockfall in Moira region, illustrating the final position of rock blocks.

2.2. Myloi Settlement

Myloi is a village of Ilia prefecture in Peloponnese, Western Greece (Figure 4). Geologically, it belongs to Olonos–Pindos and Gavrovo–Tripolis geotectonic Units and, according to the engineering geological map of Greece, is characterized primarily by Upper Cretaceous limestones (Hellenic Survey of Geology & Mineral Exploration—HSGME). Limestones with no vegetation and cherts predominate in the mountain volume above the settlement. The direction of the faults is E–W and NE–SW [40]. Various corrosion factors have severely decreased the coherence of the limestone bedrock. As a result, detachments of rock blocks and rock sliding phenomena occurred. The slope angle of these formations ranges from 45° to 60° [41].

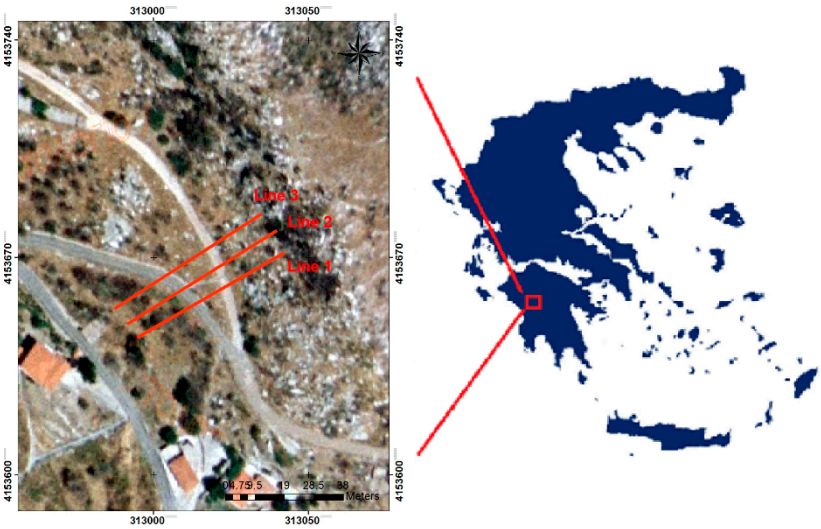

Figure 4. Slope profiles used in RocFall analysis regarding Myloi region. The slope picture is taken from Greek Cadastral (2008).

In August 2007, in the broader region of Ilia Prefecture, devastating wildfires destroyed the vegetation cover of huge areas. More than 60 people were killed, hundreds were injured and several communities were severely damaged, resulting in the loss of around 870 km^2 of mostly forest and agricultural area. Heavy rains and human activities triggered the appearance or reactivation of varying scale rockfall events, which were aided by the vegetation loss and the general sensitivity of geological formations to rockslides. Due to these wildfires, Myloi has been declared a reforestable area. On 26 January 2019, a significant rockfall occurred at Myloi settlement, near to Andritsaina town, and the volume of rock fragments displaced in Myloi rockfall on the road area and at the end of the slope profile was estimated at 147 m^3 approximately. The rockfall event is considered to be the result of the combined action of intensive rainfalls with the total absence of root system (due to the past wildfires). Those characteristics led to corrosion phenomena and, thus, the soil lost its coherence. Then, abrupt rock detachment events occurred. The debris rolled down the slope, inducing damages in two houses and to the block of the main roads at the entrance of the village (Figures 5 and 6).

Figure 5. Pictures taken from Myloi region after rockfall event.

Figure 6. Picture of the rockfall in Myloi region, illustrating the final position of rock blocks.

The aforementioned rockfall was studied via RocFall software and a 2D simulation was performed. Three slope profiles were selected (Figure 4) and extracted from eight different DSMs: one 5 cm spatial resolution DSM created by UAV field data, one 5 m DSM from the Greek Cadastral, one 20 m DSM from the Ministry of Agriculture, three 30 m resolution DEMs (ALOS AW3D30 DEM, ASTER GDEM and SRTM30 DEM) and two 90 m cell size DEMs (SRTM90 DEM and TanDEM_X). Geological and material characteristics of the slopes were derived from in situ observations and previous studies (Table 3, Figures 5 and 6) [41,42]. In the same manner as the case of Moira settlement, two barriers were added in the slope to simulate two rural roads located at x = 26 m and x = 37 m (measuring from the beginning of the slope profile), respectively.

Table 3. Geological and material characteristics.

MYLOI ROCKFALL	
Geological formation	Limestone with no vegetation
Date of the rockfall	26 January 2019
Length (m)	60
Width (m)	20
Slope profiles	3
Number of throw rocks	50
Barrier	2 roads
Coefficient of normal restitution (Rt)	Mean: 0.47/St. dev. 0.04
Coefficient of tangential restitution (Rn)	Mean: 0.85/St. dev. 0.04
Friction angle (Phi)	Mean: 10/St. dev. 2
Horizontal velocity (m/s)	Mean: 11/St. dev. 1.1

2.3. Platiana Settlement

Platiana is a village of Ilia prefecture in Peloponnese, Western Greece (Figure 7). According to the engineering geological map of Greece, it is characterized by Upper Cretaceous limestones and belongs to Pindos geotectonic Unit (Hellenic Survey of Geology & Mineral Exploration—HSGME). This large area constitutes a part of the vast Pindic Unit, which was thrusted towards the west. Large limestone outcrops (of thin and medium layer thickness) exist in the vicinity of the settlement. These limestones are locally intercalated with chert layers [41]. Corrosion factors have affected the slope and caused tensional release in the rock mass. As a result, the rocks detach from the main body and collapse.

Platiana is located 25 km away from Myloi village and also suffered the catastrophic wildfires of 2007. Since the past decade, Platiana has been declared a reforestable area. In 2008, the slope next to Platiana village was bare of vegetation, while, in 2018, after the reforestable procedures, it was converted to a verdant area (Figure 8). Heavy rainfalls led to a rockslide of one piece of rock with a mass of 10 m^3 on 4 December 2018 (Figures 9 and 10). The rock stopped in a churchyard and, luckily, no fatalities were recorded. During the rock rolling, two fences, made of drystone, were destroyed. The first fence was at the location x = 195 m and the second at x = 215 m, measuring from the beginning of the slope profile (Figure 7), with an inclination angle of about 70°.

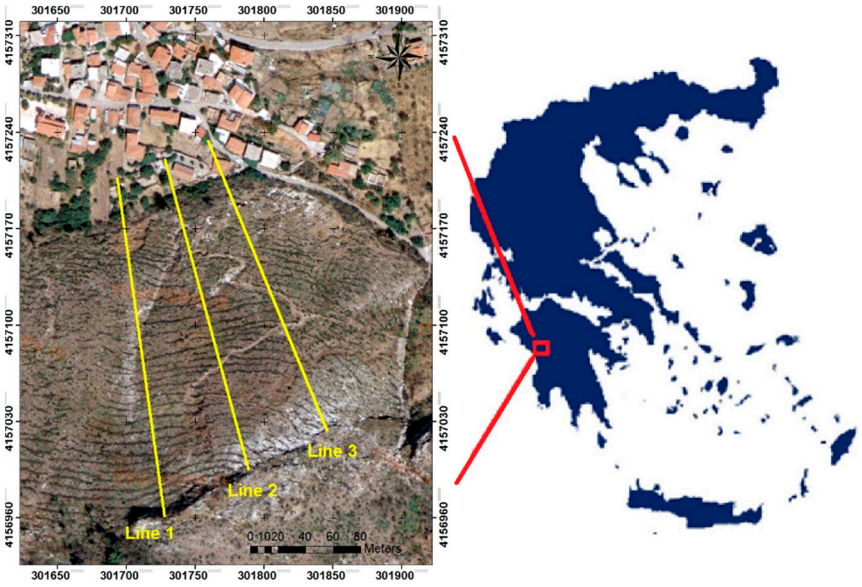

Figure 7. Slope profiles used RocFall analysis regarding Platiana region. The slope picture is taken from Greek Cadastral (2008).

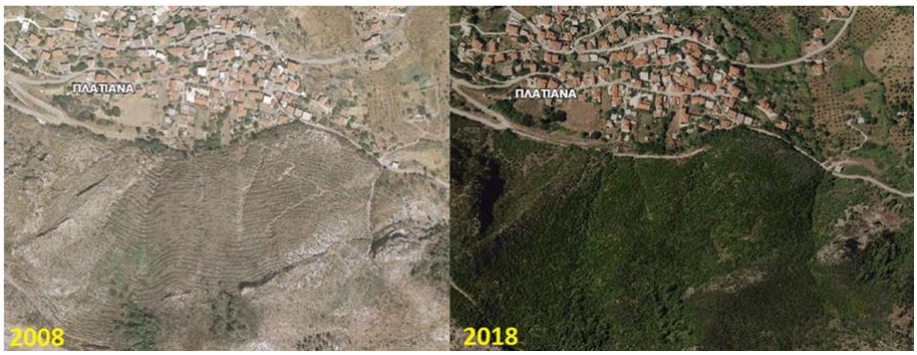

(**a**) (**b**)

Figure 8. (**a**,**b**) The slope next to Platiana village before and after the reforestation procedures.

Figure 9. Pictures taken from Platiana region after rockfall event.

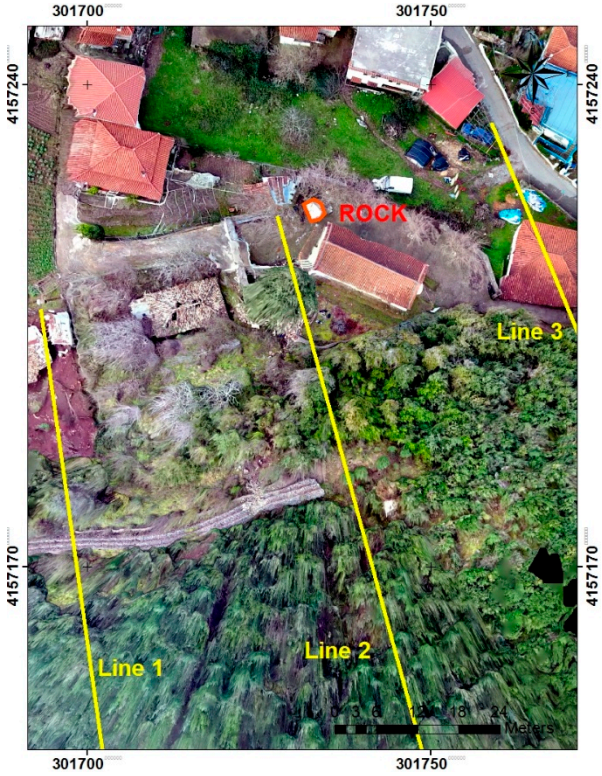

Figure 10. Picture of the rockfall in Platiana region, illustrating the final position of the rock.

For examining this particular rockfall phenomenon, three slope profiles were selected (Figure 7) and extracted from eight different DSMs, aiming at a 2D simulation via RocFall software: one 5 cm spatial resolution DSM created by UAV data, one 5 m DSM from the Greek Cadastral, one 20 m DSM from the Ministry of Agriculture, three 30 m resolution DEMs (ALOS AW3D30 DEM, ASTER GDEM and SRTM30 DEM) and two 90 m cell size DEMs (SRTM90 DEM and TanDEM_X). The two aforementioned barriers, drystone fences, were taken into account in software settings, as well as geological and material characteristics of the slope profiles (Table 4). In situ surveys and literature data were accomplished (Figures 9 and 10) [40,41,43].

Table 4. Geological and material characteristics.

PLATIANA ROCKFALL	
Geological formation	Limestone with dense vegetation
Date of rockfall	4 December 2018
Length (m)	240
Width (m)	120
Slope profiles	3
Number of throw rocks	1
Barrier	2 fences
Coefficient of normal restitution (Rt)	Mean: 0.39/St. dev. 0.04
Coefficient of tangential restitution (Rn)	Mean: 0.8/St. dev. 0.04
Friction angle (Phi)	Mean: 15/St. dev. 2
Horizontal velocity (m/s)	Mean: 11/St. dev. 1.1

3. Software and Materials

For this investigation, RocFall 4.0 from Rocscience was used, which is a two-dimensional rockfall modeling tool for steep slopes. The detection of rockfall susceptibility is achieved through a lumped mass statistical analysis. Protective measures can be easily identified by modifying the material properties of each slope segment and, if necessary, changing the material. The materials from which the slope consists of might differ significantly from one part to another [44]. Slopes also exhibit large anomalies with their geometry. A numerical analysis, via RocFall, may be rerun with new data, and the findings can be compared to the prior ones. This software comprises the collision theory and Newton's laws of motion, so as to simulate the path of the rolling rock mass/boulder [45].

RocFall software calculates four parameters for the entire slope, including the final position of the rock, bounce height and velocity, as well as energies. For the first parameter, "rock ends" is the terminus or the point at which the falling rock will halt. The correct and accurate computation of this factor is critical for the hazard mapping, since natural or human-caused disasters can be prevented. The second parameter, "bounce height", is influenced by slope gradient, slope geometry, size and shape of the failure rock blocks and is one of several significant elements in landslide assessment [46]. The computation of the third parameter, "velocity", is also affected by slope geometry and establishes an important step towards the determination of potential catastrophic events [47]. Changing elevation measurements, along the under-review trajectory, leads to serious discrepancies of the calculated velocity. Last but not least, the kinetic energy is described by the produced energy of a falling and driven-by-gravity rock. The existence of barriers (roads, fences, buildings and vegetation) along a slope profile affects all the aforementioned parameters. The software's data collector processes the input factors and a multiparameter rockfall simulation is presented.

Slope definition, slope material definition, materials to the slope segment assignment, rock starting location determination, analysis computation and graph of the results are parts of RocFall software analysis. The creation of slope profiles was accomplished in ArcGIS environment and the produced slope lines were introduced in RocFall simulation program. In this study, three slope profiles for each area of interest, Moira, Myloi and Platiana settlements, were selected. Eight different DSMs with spatial resolution ranging from 5 cm to 90 m were used for the extraction of the slope profiles. More specifically, these DSMs are UAV DSM, DSM taken from the Greek Cadastral, DSM from the Ministry of Agriculture, ALOS AW3D30 DEM, ASTER GDEM, SRTM30 DEM, SRTM90 DEM and TanDEM_X. The outcome of the rockfall simulation is affected by the roughness of the slopes. Hence, the determination of roughness is necessary and is easily gained via remote sensing techniques. Furthermore, slopes' geological features influence the output of the rockfall simulation, a fact that has been taken into consideration. Energy loss is recorded due to the before-mentioned characteristics and depends on the type of the trajectory [48].

For the accurate simulation of rock blocks' movement, the RocFall software for each imported slope profile considers constant values of both coefficient of normal restitution (Rn) and coefficient of tangential restitution (Rt). Furthermore, the software does not allow the user to manually alter the above coefficients [8]. The constant value of these coefficients is supported by the PhD thesis of N. Vagenas (2020) [41], who performed laboratory tests, emphasizing those three rockfall events mentioned before, directed by the Laboratory of Engineering Geology of the University of Patras, Greece.

In addition, the determination of input parameters for a RocFall analysis includes the type of soil/rock and the vegetation of the area of interest. More specifically, the tool "material editor" has some fixed options, such as asphalt, bedrock outcrops, clean hard bedrock, soil with vegetation, talus cover and talus with vegetation [8]. These fixed options correspond to default values for the coefficient of normal and tangential restitution, friction angle and slope roughness. In this work, additional types/materials were chosen, as the default options were not appropriate. The aforementioned materials are available for each study area presented in Section 3.

Last but not least, according to RocFall software, roads can be simulated as barriers [8] and, since roads do exist in the under-study rockfall regions, they have been taken into consideration in order for the software to ponder the topographic conditions in a more realistic manner. These roads have a notable impact on the under-study rockfall events, since they create discontinuities and zero-inclination surfaces on the slopes. Consequently, as is observed either numerically or by in situ observations, a vast number of rocks stop upon these road/barriers.

4. Results

4.1. Moira Rockfall Simulation

The initial step for the simulation of Moira rockfall, via RocFall software, was the creation of the slope profiles. These profiles were extracted from seven different DSMs and led to the depiction of slope geometry. A barrier, in the form of a road inside the rockfall body, at the location x = 128 m was taken into account, as it affects the slide of the rock block and impacts the software calculations. In the following pictures, 2D rockfall simulations of 50 rocks, pertaining to Moira rockfall, are presented and correspond to the second slope profile (Figure 11).

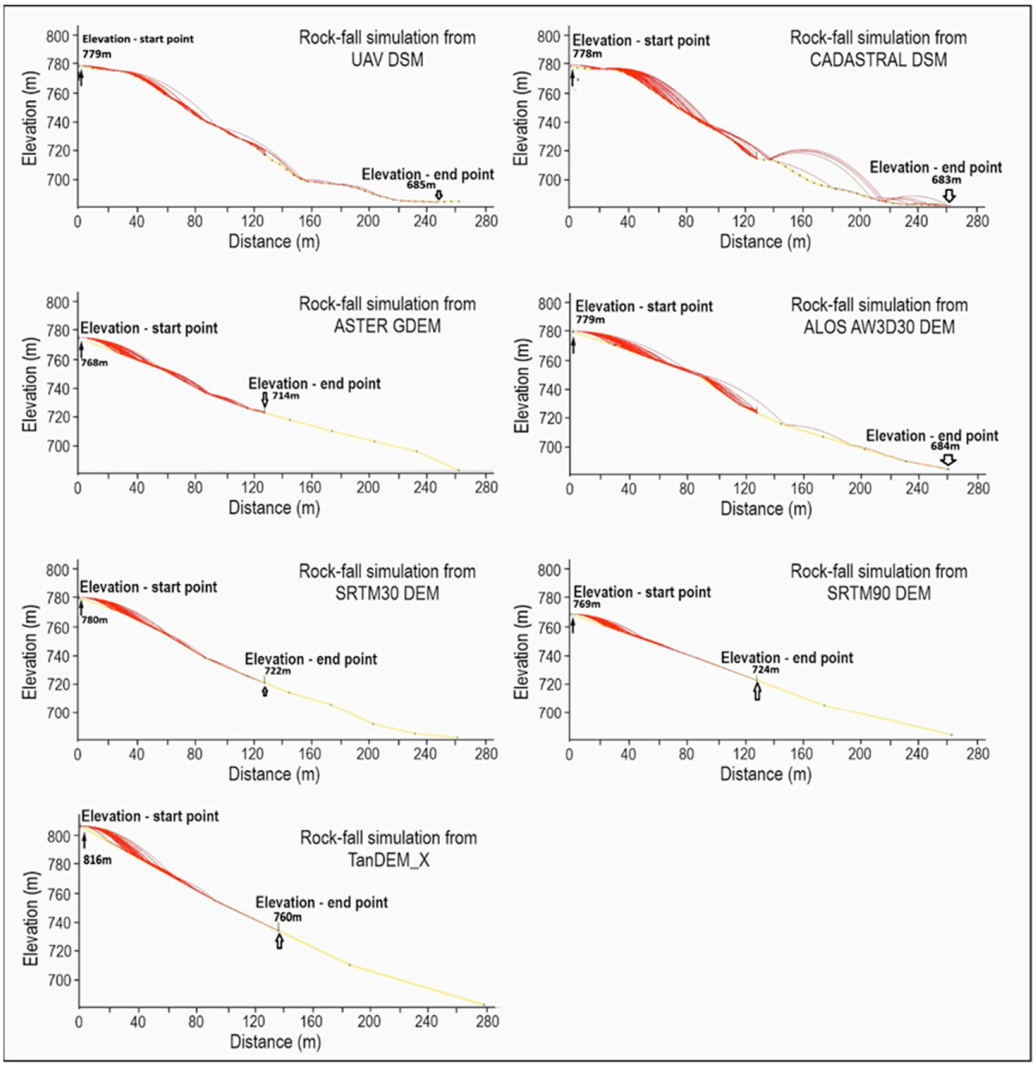

Figure 11. Two-dimensional rockfall simulations via RocFall software for the 2nd slope profile.

Graph depiction divergence depends on the used DSMs for the creation of the slope profiles. It is observed that UAV DSM and DSM from the Greek Cadastral designed a

detailed topography by altering steep slopes and smooth areas. On the other hand, the other DSMs, with coarse spatial resolutions, tended to flatten the topography and create uniform areas throughout the length of the slope. The relief of the area holds key information for the rockfall simulation, as it affects the motion of the rock, either by bouncing or by rolling. UAV DSM, DSM from the Greek Cadastral and ALOS AW3D30 DEM profiles presented rocks bouncing, while ASTER GDEM, SRTM30 DEM, SRTM90 DEM and TanDEM_X illustrated only rocks rolling. According to the in situ observations, some rocks crossed the road (barrier) and reached the end of the slope profile. Consequently, UAV DSM, DSM from the Greek Cadastral and ALOS AW3D30 DEM best simulate the real rockfall trajectory. Rockfall simulations based on ALOS AW3D30 DEM show that just one rock overcomes the barrier (road). This result opposes the in situ measurements, which recorded a plethora of rocks at the lower slope (Figure 3). The horizontal location of rock end points was also calculated, with the purpose of presenting the precise location of rock stop points from each DSM profile (Table 5, Figure 12).

Table 5. Horizontal location of rock end points for the 2nd slope profile.

Slope Profile 2 BARRIER ROAD AT X = 128 m		
	Min. Location (m)	**Max. Location (m)**
UAV DSM	128.20	248.56
CADASTRAL DSM	127.98	258.56
ASTER GDEM	127.97	127.97
ALOS_AW3D30 DEM	127.85	258.35
SRTM 30 DEM	127.80	127.80
SRTM 90 DEM	128.04	128.04
TANDEM_X	127.86	127.86

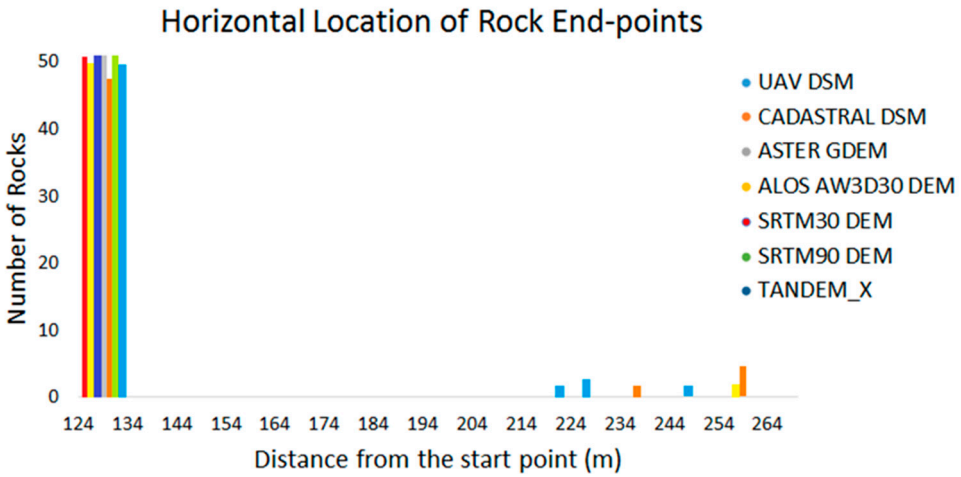

Figure 12. Horizontal location of rock end points for the 2nd slope profile.

The UAV DSM slope profile indicated that the rocks stopped at four sites. The first was at the location x = 128.20 m (the point of the barrier/road), the second at x = 222.39 m, the third at x = 227.62 m and the fourth at x = 248.56 m (which is almost at the end of the slope profile). The DSM from the Greek Cadastral depicted three end points, at x = 127.98 m, at x = 237.67 m and at x = 258.56 m. The ALOS AW3D30 DEM presented two end points, at the barrier (x = 127.85 m) and at the end of the slope (x = 258.35 m). Based on the rest of the DSMs, the boulders end up at the barrier/road that is located at x = 128 m. The horizontal location of rock end points is in conjunction with the type of slope; hence, smoother slope profiles (ASTER GDEM, SRTM30 DEM, SRTM90 DEM and TanDEM_X) force the rocks to

stop at the barriers. A common observation is that all the DSMs stopped the majority of the rocks in the position of the barrier–road.

The bounce height was calculated as a function of (i) the height above the slope (m), (ii) the horizontal location (m) and (iii) the number of bounces (Table 6, Figure 13).

Table 6. Bounce height for the 2nd slope profile.

Slope Profile 2	BARRIER ROAD AT X = 128 m		
	Max. Height above Slope (m)	**Horizontal Location (m)**	**Number of Bounces**
UAV DSM	6.26	125.36	4
CADASTRAL DSM	23.06	260	5
ASTER GDEM	6.26	125.36	4
ALOS_AW3D30 DEM	10.35	260	4
SRTM 30 DEM	5.13	125.18	4
SRTM 90 DEM	4.66	78.38	2
TANDEM_X	7.01	125.02	2

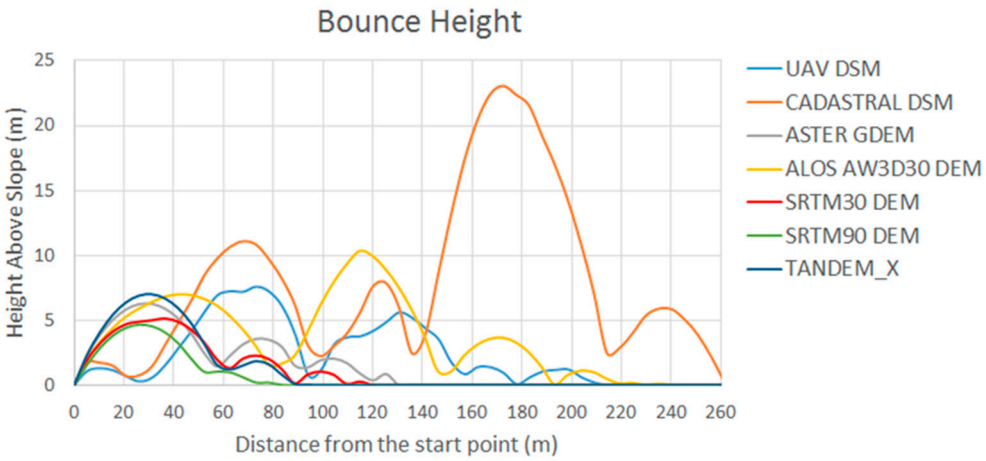

Figure 13. Bounce height for the 2nd slope profile.

The rocks in the slope profiles created by UAV DSM, DSM from the Greek Cadastral and ALOS AW3D30 DEM jumped along the relief without rolling, and the horizontal location of rock end points was at the end of the slope, whereas ASTER GDEM, SRTM30 DEM, SRTM90 DEM and TanDEM_X exhibited two to four rock bounces approximately, with height above the slope less than 7.5 m (in the beginning of the slope profiles), and then rolled until their kinetic energy reduces to zero. The above is logical, as the DSMs with spatial resolution over 30 m illustrated the reliefs more smooth and flat, where rocks just rolled. On the other hand, the steep slopes from DSMs with high cell size led to rock bounces in the unsmooth areas.

The computation of the total kinetic energy distribution was accomplished in the middle of the slope profile at the location x = 130 m (Table 7, Figure 14).

Table 7. Total kinetic energy distribution at x = 130 m for the 2nd slope profile.

Slope Profile 2	**BARRIER ROAD AT X = 128 m**			
	Min. Kinetic Energy (kJ)	**Max. Kinetic Energy (kJ)**	**Slope Degrees**	**Number of Rocks**
UAV DSM	42.12	62.18	40.13	4
CADASTRAL DSM	58.22	65.74	21.95	5
ASTER GDEM	0	0	16.41	0
ALOS_AW3D30 DEM	71.61	71.61	29.54	1
SRTM 30 DEM	0	0	23.42	0
SRTM 90 DEM	0	0	20.96	0
TANDEM_X	0	0	20.01	0

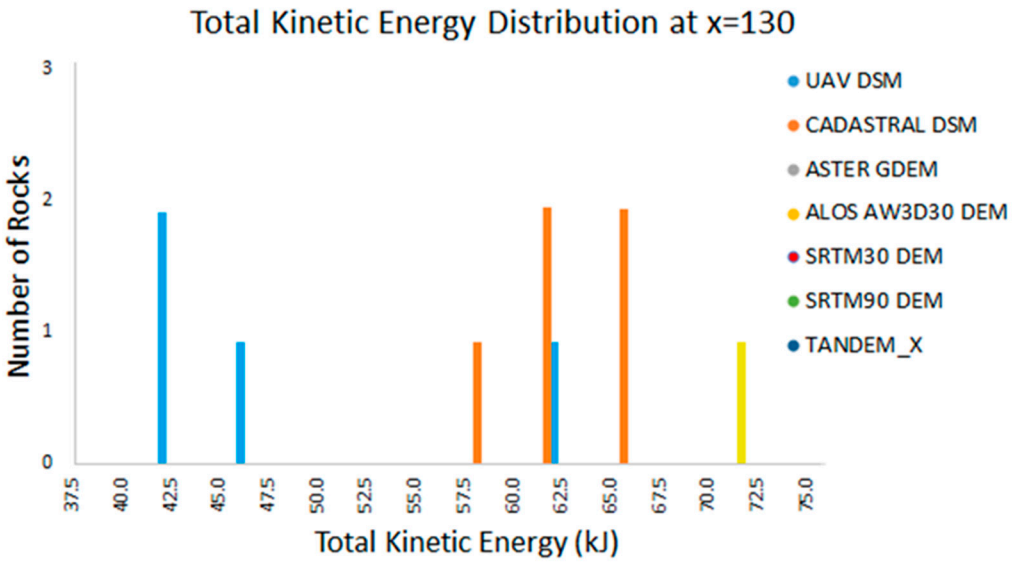

Figure 14. Total kinetic energy distribution at x = 130 m for the 2nd slope profile.

The UAV DSM, DSM from the Greek Cadastral and ALOS AW3D30 DEM recorded total kinetic energy distribution at x = 130 m ranging from 42 kJ to 71 kJ. These kinetic energy values are due to the bouncing phenomena. When the rocks in the slope profiles created by the aforementioned DSMs jumped, as in the previous diagrams presented, they then developed high speed and, consequently, the software computed high kinetic energies. On the other hand, for the rest of the DSMs, the total kinetic energies were not calculated, as the rocks stopped at the barrier (x = 128 m).

4.2. Myloi Rockfall Simulation

In Myloi rockfall, eight DSMs with spatial resolutions ranging from 5 cm to 90 m were used for the extraction of three slope profiles. In reference to Moira study area, we disposed an additional DSM created from aerial photos by the Ministry of Agriculture. The specific DSM has a spatial resolution of 20 m. RocFall software simulated the motion of 50 rocks. Two barriers, in the form of local roads, were added at the position x = 26 m and at x = 37 m. In the following pictures, the 2D rockfall simulations are presented and correspond to the second slope profile (Figure 15).

According to the figures above, the UAV DSM produced the most detailed slope profiles, with steep slopes, which led to many rock jumps and plenty of rock rollings until a number of them reached the end of the slope. The DSM from the Greek Cadastral, DSM from the Ministry of agriculture and ALOS AW3D30 DEM created slopes smoother than the UAV DSM. In these cases, also, some rocks jumped and reached the end. The rest pf the DSMs flattened the line of the slope and the rocks stopped in the first barrier at the

location x = 26 m. So, the higher the spatial resolution of the DSM, the more accurate the slope depiction. Based on the in situ observations, the rocks overcame the barriers/roads and stopped at the end of the relief. Thus, it is proved that only UAV DSM, DSM from the Greek Cadastral, DSM from the Ministry of agriculture and ALOS AW3D30 DEM achieved a rockfall simulation close to real conditions.

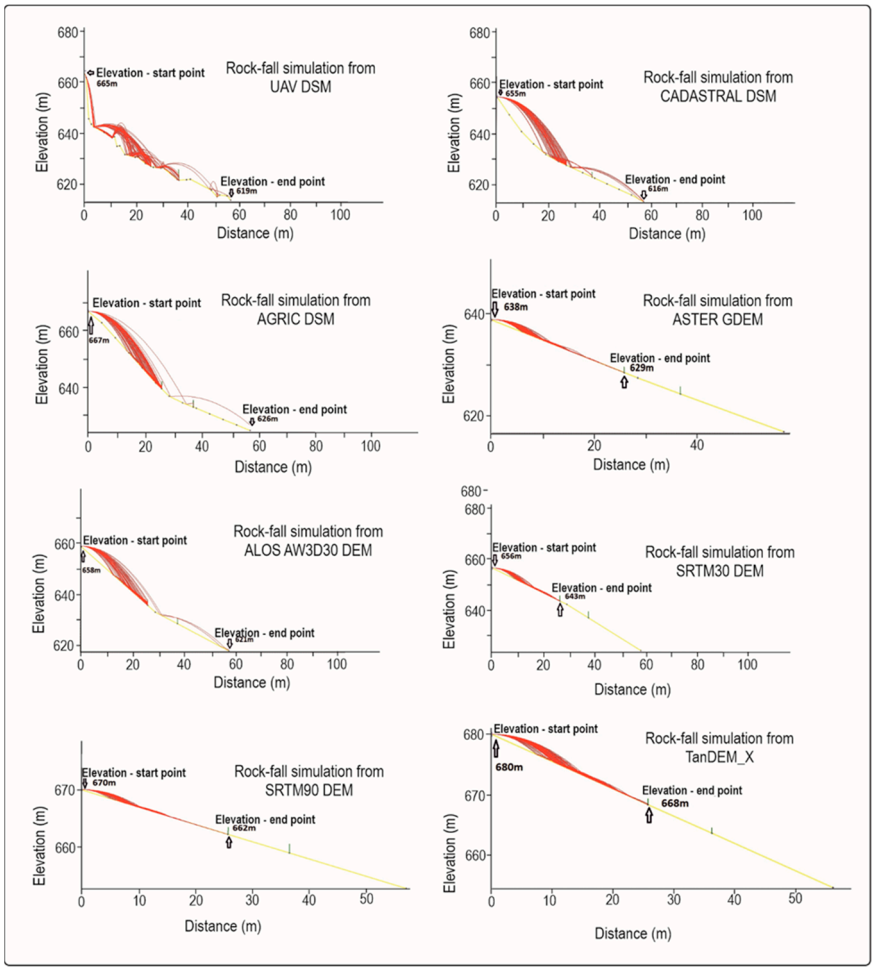

Figure 15. Two-dimensional rockfall simulations via RocFall software for the 2nd slope profile.

The extracted end points of the rock trajectories are presented in the following table (Table 8, Figure 16) and correspond to the second slope profile of Myloi settlement.

Table 8. Horizontal location of rock end points for the 2nd slope profile.

Slope Profile 2	**BARRIER ROAD 1 AT X = 26 m and ROAD 2 AT X = 37 m**	
	Min. Location (m)	**Max. Location (m)**
UAV DSM	25.58	56.25
CADASTRAL DSM	26.86	56.28
DSM AGRIC.	26.12	56.37
ASTER GDEM	25.59	25.59
ALOS_AW3D30 DEM	26.23	56.41
SRTM 30 DEM	26.05	26.05
SRTM 90 DEM	25.95	25.95
TANDEM_X	25.62	25.62

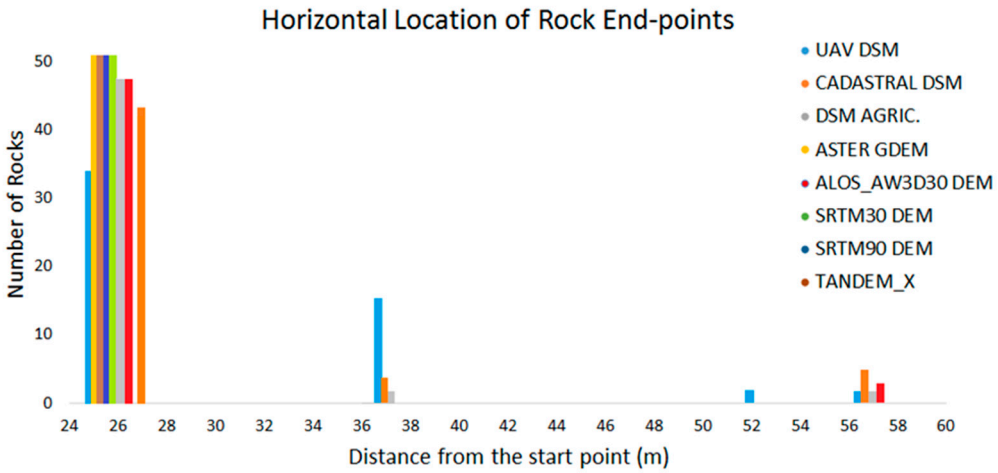

Figure 16. Horizontal location of rock end points for the 2nd slope profile.

The results of the above figures indicated that, via the use of UAV DSM slope profile for rockfall simulation, the rocks stopped at four different points. The first point was a few centimeters before the first barrier/road at x = 25.58 m (where almost 33 rocks stopped), the second point was at the second barrier/road at x = 37.10 m (15 rocks stopped), the third at the location x = 51.93 m and the fourth at x = 56.25 m. The rocks that simulated from the DSM from the Greek Cadastral and from the DSM from the Ministry of Agriculture showed three end points, which are the two barriers/roads and the end of the slope profile, while, from ALOS AW3D30 DEM slope profile, the rocks stopped at the first barrier/road and at the end of the slope. From ASTER GDEM, SRTM 30 DEM, SRTM 90 m DEM and TanDEM X simulation, the rocks' trajectory stopped at the first barrier.

The bounce height was also simulated and the results of the second slope profile are presented below (Table 9, Figure 17).

Table 9. Bounce height for the 2nd slope profile.

Slope Profile	**BARRIER ROAD 1 AT X = 26 m and ROAD 2 AT X = 37 m**		
	Max. Height above Slope (m)	**Horizontal Location (m)**	**Number of Bounces**
UAV DSM	12.17	59.07	4
CADASTRAL DSM	11.43	59.13	2
DSM AGRIC.	10.12	59.18	2
ASTER GDEM	1.08	22.74	3
ALOS_AW3D30 DEM	6.79	57.18	2
SRTM 30 DEM	2.09	25.15	2
SRTM 90 DEM	0.9	18.25	2
TANDEM_X	1.81	25.05	2

Bounce height diagrams showed that the rocks in the slope profiles created by ASTER GDEM, SRTM30 DEM, SRTM90 DEM and TanDEM_X mainly rolled or jumped the slope and stopped before the first barrier in horizontal locations less than 26 m. The number of bounces ranged from two to three and the height above slope was between 0.9 m and 2.09 m. On the other hand, in the DSMs with high spatial resolution (UAV DSM, DSM from the Greek Cadastral, DSM from the Ministry of Agriculture and ALOS AW3D30 DEM), the rocks jumped along the slope profile until they reached the end of the slope. The height above slope ranged from 6.79 m to 12.17 m. The maximum number of bounces was recorded by the UAV DSM simulation.

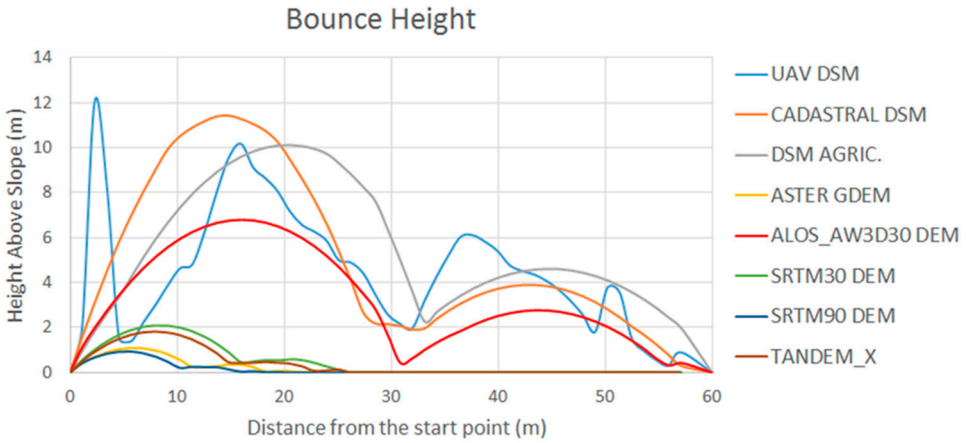

Figure 17. Bounce height for the 2nd slope profile.

In the following step, the total kinetic energy was calculated in the middle of the slope profile (x = 28.5 m) (Table 10, Figure 18).

Table 10. Total kinetic energy distribution at x = 28.5 m for the 2nd slope profile.

Slope Profile 2	BARRIER ROAD 1 AT X = 26 m and ROAD 2 AT X = 37 m			
	Min. Kinetic Energy (kJ)	Max. Kinetic Energy (kJ)	Slope Degrees	Number of Rocks
UAV DSM	13.62	106.24	88.86	17
CADASTRAL DSM	71.15	163.23	24.09	7
DSM AGRIC.	157.33	177.63	37.45	2
ASTER GDEM	0	0	21.46	0
ALOS_AW3D30 DEM	146.41	154.77	26.76	2
SRTM 30 DEM	0	0	29.24	0
SRTM 90 DEM	0	0	19.98	0
TANDEM_X	0	0	21.02	0

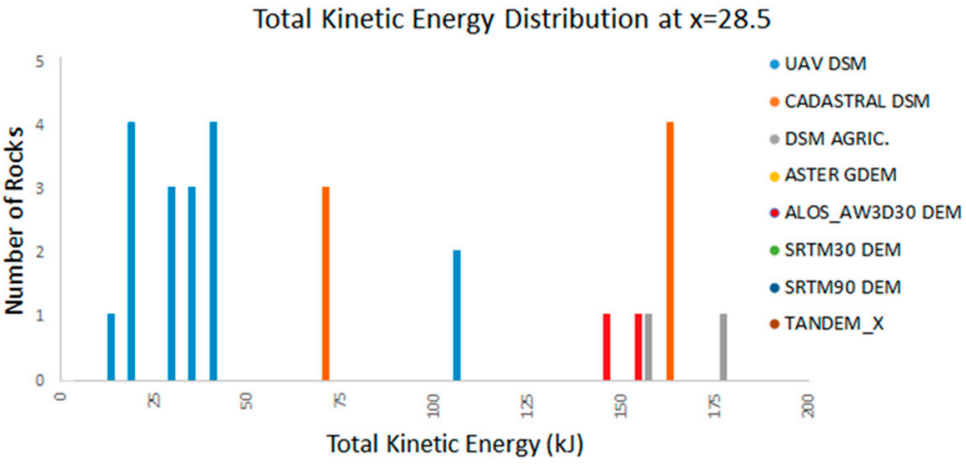

Figure 18. Total kinetic energy distribution at x = 28.5 m for the 2nd slope profile.

The total kinetic energy was computed in the middle of the slope profile at the location x = 28.5 m. This position is after the first barrier/road (x = 26 m) and before the second (x = 37 m). According to the diagram "horizontal location of rock end points", in ASTER GDEM, SRTM30 DEM, SRTM90 DEM and TanDEM_X slope profiles, the rocks stopped at the first barrier/road (x = 26 m). Consequently, at the location x = 28.5 m, the number of rocks was zero and, thus, there was no kinetic energy. In contrast, in the UAV DSM, DSM

from the Greek Cadastral, DSM from the Ministry of Agriculture and ALOS AW3D30 DEM profiles, a number of rocks reached the end of the slope profiles; therefore, kinetic energy was recorded. From DSM from the Ministry of Agriculture simulation, two rocks were calculated with maximum kinetic energy equal to 177 kJ. The kinetic energies of seventeen rocks were computed by the UAV DSM slope profile, seven rocks by the DSM from the Greek Cadastral slope profile and two rocks by the two ALOS AW3D30 DEM.

4.3. Platiana Rockfall Simulation

Eight DSMs with spatial resolutions ranging from 5 cm to 90 m were used for the extraction of three slope profiles in Platiana rockfall. In this case, only one large rock was simulated instead of fifty rocks that were inserted in the previous examples. The mass of the rock was over 10 m^3. Two barriers, drystone fences, were taken into account at the position x = 195 m and at x = 215 m. Two-dimensional rockfall simulations are presented in the following figures and correspond to the second slope profile (Figure 19).

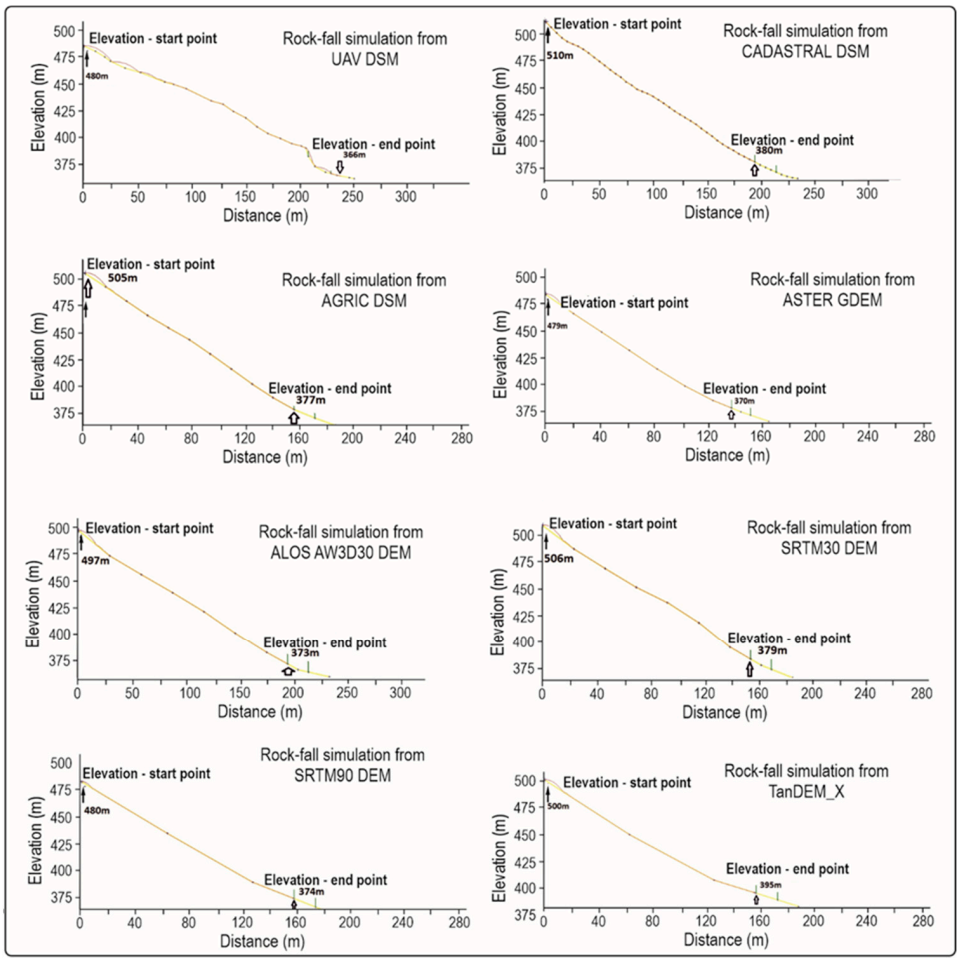

Figure 19. Two-dimensional rockfall simulations via RocFall software for the 2nd slope profile.

According to the figures above, only the UAV DSM created a detailed slope profile, with steep slopes and smooth areas. The other DSMs tended to flatten the topography. The rock in the UAV DSM slope profile jumped the first barrier/fence and broke the second barrier/fence. This result, in comparison with the field observations, is reliable, as the rock stopped a few meters before the end of the slope, in the churchyard (Figure 9). In the DSM from the Greek Cadastral, DSM from the Ministry of Agriculture, ALOS AW3D30 DEM, ASTER GDEM, SRTM30 DEM, SRTM90 DEM and TanDEM_X slope profiles, the rock rolled and stopped in the first barrier/fence. This is in contrast to the real trajectory. Therefore, only the UAV DSM simulated a trajectory close to the real.

The end point of the rock was calculated and presented in the next step. The following figures correspond to the second slope profile of Platiana settlement (Table 11, Figures 20 and 21).

Table 11. Horizontal location of rock end points for the 2nd slope profile.

Slope Profile 2	BARRIERS FENCE 1 AT X = 195 m and FENCE 2 AT X = 215 m	
	Min. Location (m)	Max. Location (m)
UAV DSM	223.45	223.45
CADASTRAL DSM	194.76	194.76
DSM AGRIC.	194.73	194.73
ASTER GDEM	194.21	194.21
ALOS_AW3D30	194.56	194.56
SRTM 30 DEM	194.35	194.35
SRTM 90 DEM	195.24	195.24
TANDEM_X	194.42	194.42

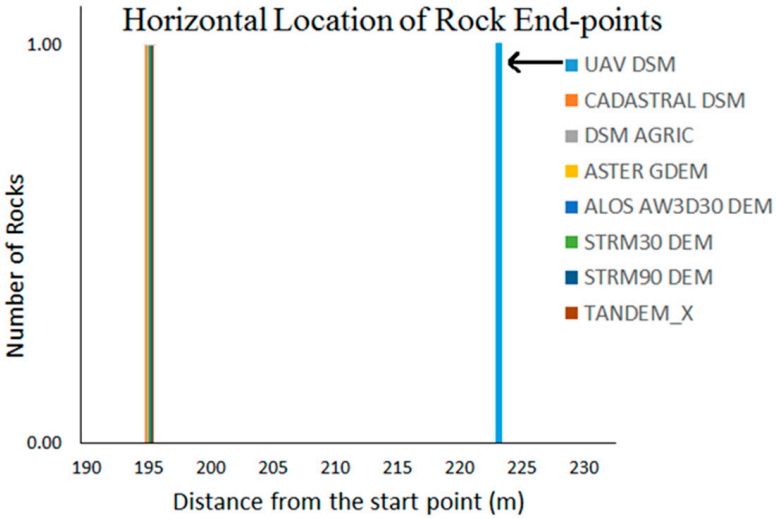

Figure 20. Horizontal location of rock end points for the 2nd slope profile from all the DSMs.

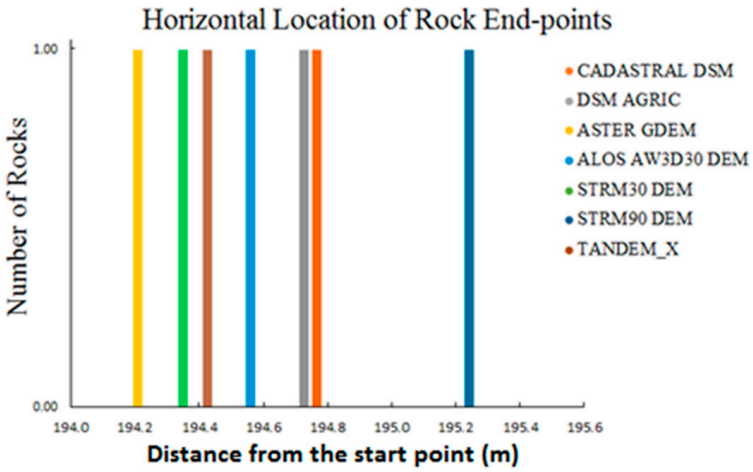

Figure 21. Horizontal location of rock end points for the 2nd slope profile from all the DSMs, except from UAV DSM.

Figure 20 shows that the rock simulated by the UAV DSM slope profile stopped at the location x = 223.45 m, crossing the two barriers/fences and stopping a few meters before the end of the slope. The simulation by the DSM from the Greek Cadastral, DSM from the Ministry of Agriculture, ALOS AW3D30 DEM, ASTER GDEM, SRTM30 DEM, SRTM90 DEM and TanDEM_X indicated the horizontal location of rock end point approximately as x = 195 m (Figure 21). This location was the first barrier/fence.

The bounce height also simulated and the results of the second slope profile are presented below (Table 12, Figure 22).

Table 12. Bounce height for the 2nd slope profile.

Slope Profile 2	**BARRIERS AT X = 195 m and AT X = 215 m**		
	Max. Height above Slope (m)	**Horizontal Location (m)**	**Number of Bounces**
UAV DSM	3.79	211.68	5
CADASTRAL DSM	0.054	154.87	3
DSM AGRIC.	3.91	98.53	1
ASTER GDEM	3.32	28.07	2
ALOS_AW3D30	3.4	18.75	1
SRTM 30 DEM	4.07	177.95	2
SRTM 90 DEM	1.7	164.66	2
TANDEM_X	2.93	163.97	2

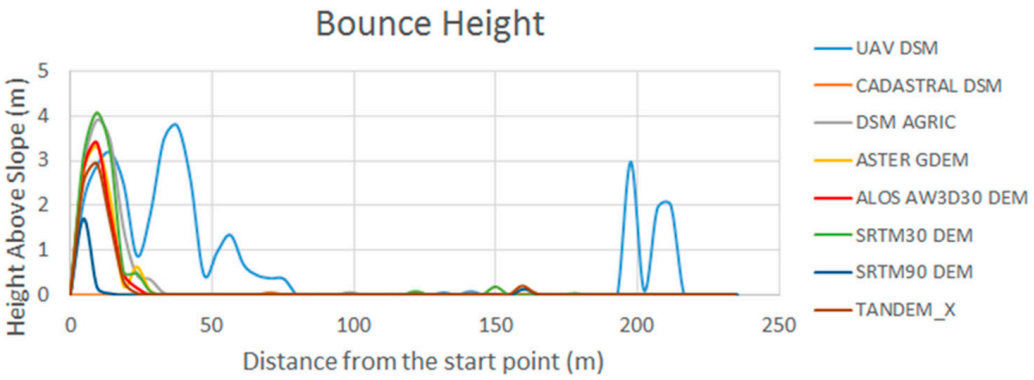

Figure 22. Bounce height for the 2nd slope profile.

The bounce height diagram from UAV DSM slope profile showed three rock jumps during the first 80 m of the slope. Then, the rock rolled further for 110 m, after bouncing twice, and finally stopped at x = 224. The rock simulation by the DSM from the Greek Cadastral profile illustrated only rock rolling without jumping. In the DSM obtained from the Ministry of Agriculture, ASTER GDEM, ALOS AW3D30 DEM, SRTM30 DEM, SRTM90 DEM and TanDEM_X slope profiles, the rock initially jumped once/twice in the first 30 m and then rolled until it stopped in different horizontal locations. UAV DSM, DSM from the Ministry of Agriculture, ASTER GDEM, ALOS AW3D30 DEM and SRTM30 DEM recorded maximum height above slope over 3 m.

The total kinetic energy distribution was computed in the middle of the slope profile, at x = 117.3 m, and is presented below (Table 13, Figure 23).

Table 13. Total kinetic energy distribution at x = 117.3 m for the 2nd slope profile.

Slope Profile 2	BARRIERS FENCE 1 AT X = 195 m and FENCE 2 AT X = 215 m		
	Total Kinetic Energy (kJ)	Slope Degrees	Number of Rocks
UAV DSM	17.24	75.72	1
CADASTRAL DSM	88.94	35.59	1
DSM AGRIC.	370.78	33.82	1
ASTER GDEM	710.61	30.26	1
ALOS_AW3D30 DEM	541.79	33.5	1
SRTM 30 DEM	367.41	29.73	1
SRTM 90 DEM	726.44	30.9	1
TANDEM_X	593.02	30.8	1

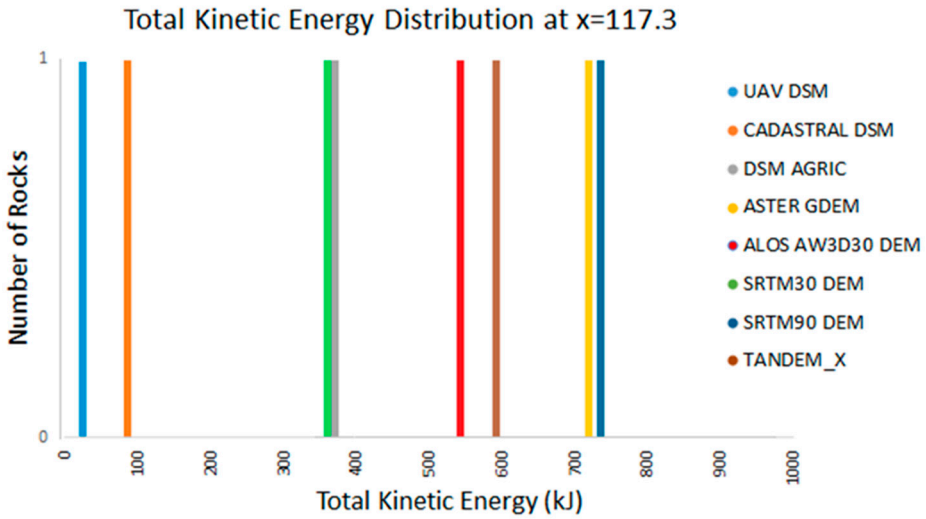

Figure 23. Total kinetic energy distribution at x = 117.3 m for the 2nd slope profile.

From Figure 23, it is observed that the rock that participated in the Platiana rockfall event demonstrated low kinetic energy values when slope profiles derived from UAV DSM and DSM from the Greek Cadastral are used. In contrast, medium kinetic energy values are produced from the DSM from the Ministry of Agriculture, ALOS AW3D30 DEM and SRTM30 DEM and high kinetic energy values corresponded to ASTER GDEM, SRTM90 DEM and TanDEM_X. So, the DSMs with coarser spatial resolution (more than 30 m) flattened the relief; consequently, the rock recorded higher speed than in the other DSMs with high spatial resolution (less than 30 m), which created unsmooth surfaces.

5. Discussion

Rockfall investigations are carried out to evaluate the hazard and mitigate the risk of rockfall events. As in the study areas, rockfall occurred near to roads; hence, the assessment of rockfall risk along roads has been widely studied [49–51]. Remote sensing techniques contribute to this research, offering advantages such as minimization of data collection time, contrary to in situ observations, data acquisition in inaccessible areas and, sometimes, limitation of research expenditures. The purpose of this study was to determine the level at which spatial resolution of DSMs may affect rockfall simulations. Data obtained from these three different rockfall events were extracted and compared with each other and/or with previous studies. In particular, the correlation between the spatial resolution of the DSM and the extent of the rockfall and the existence or not of vegetation are examined and discussed below.

In general, a plethora of rockfall/landslide investigations have been accomplished in the last 30 years via remote sensing techniques. DSMs with spatial resolutions ranging from 0.3 m to 200 m have been used in rockfall/landslide surveys [52]. Some of the used DSMs in this study, such as DSM from the Greek Cadastral, ALOSAW3D30 DEM, ASTER GDEM, SRTM30 DEM, SRTM 90DEM and TanDEM_X, have also been selected for rockfall mapping by other researchers. More specifically, Kawabata et al. (2009); Oh et al. (2013); Fuchs et al. (2014); Mahalingam et al. (2016); Rasyid et al. (2016); Wang et al. (2016); Pradhan et al. (2017) and Juliev et al. (2019) selected ASTER GDEM in their studies, which pertain to medium-scale landslides events [53–60]. Moreover, SRTM 30DEM was chosen by Mclean (2011) and Fenton et al. (2013) for medium-scale occurrences [61,62]. On the other hand, for large-scale rockfall/landslides, Calvello et al. (2013) and Huang et al. (2014) preferred the use of SRTM 90DEM [63,64]. Nowadays, DSMs with 90 m cell size are sparsely used in rockfall studies. Kakavas et al. (2021) summarized previous research in a review paper pertaining to the use of DSMs in the study of rockfalls and landslides [52]. According to the specific review, only 6% of the published (eight studies, namely [63–70]) used DSM with coarser resolution than 90 m. In the current paper, 90 m DSMs were selected in order to check the reliability of their results. The outcome was that 90 m DSMs are not reliable in rockfall/landslide investigations and the previous studies should be revised.

The current study examined three rockfall events with extents varying from 20 m width (Myloi) to 120 m width (Platiana) and from 60 m length (Myloi) to more than 260 m (Moira). At the same time, the spatial resolution of the used DSMs varies between 5 cm and 90 m. As it was proved in all the cases as the spatial resolution ameliorates, the rockfall simulation becomes more realistic. In all the studied areas, the DSMs with the higher spatial resolution (UAV, Cadastral and Ministry of Agriculture DSM) produced better results than the DSMs with the coarser spatial resolution, such as ASTER GDEM or SRTM DEM. In the case of Moira and Myloi rockfalls, the simulations from the UAV DSM and DSM of Greek Cadastral are in line with the in situ observations. Especially in Myloi case, the DSM from the Ministry of Agriculture also simulated rockfall trajectories close to the real event. ASTER GDEM, SRTM30 DEM, SRTM90 DEM and TanDEM_X are not trustworthy since, according to the rockfall simulations, all the rocks should stop at the barriers/roads. The outcomes from the Platiana rockfall study were slightly different compared to the other two cases. In this case only the UAV DSM offered a simulation the same as the real one. The huge rock penetrated through the two barriers/drystone fences and stopped in the churchyard. The slope profile created by UAV DSM illustrated the aforementioned trajectory. According to the simulations derived by the rest of the DSMs (DSM from the Greek Cadastral, DSM from the Ministry of Agriculture, ALOS AW3D30 DEM, ASTER GDEM, SRTM30 DEM, SRTM90 DEM and TanDEM_X), the rock stopped rolling at the first barrier/fence. These results differ from the field observations. Consequently, only UAV DSM offered a realistic trajectory.

These results are in accordance with previous studies. A previous similar study [62] determined how the resolution of DEMs affects regional landslide probability and concluded that, for each DEM, the ability to accurately reflect the nature of the terrain is directly related to the DEM cell size. As the size of the cell increases, the representation of the terrain's true roughness becomes less accurate [62]. In rockfall investigations, the use of DSMs with spatial resolution over 50 m is not preferable due to the low accuracy [71]. The resampling of a large pixel size into a smaller one offers a more detailed depiction of the topography. Kakavas et el. (2021) composed a literature review for the effect of DEM resolution on rockfalls and concluded that only 1% of the researchers chose DSMs with resolution over 50 m in their studies, while the majority used DSMs with resolution less than 10 m [52]. Consequently, DSMs with low spatial resolution are not appropriate in rockfall investigations according to the literature. Moreover, Wechsler (2007) and Wechsler and Kroll (2006) have recognized uncertainty and errors associated to DEMs and their propagation into derivative terrain variables and have given recommendations to overcome the problem, which is particularly relevant where the morphometric variables are derived from

a DEM acquired after the occurrence of the slope failures [72,73]. High-resolution DSMs should be preferred in regional-scale events, while coarse cell sizes should be preferred in large-scale rockfall zones, as these affect the reliability of rockfall simulation programs [74].

Regarding the areas of interest, having extracted slope profiles from eight different DSMs with spatial resolutions ranging from 5 cm to 90 m, it is observed that the DSMs with high spatial resolution led to more accurate slope depiction, while those with coarse spatial resolution lose a circumstantial illustration. High-resolution models calculate acute slope angles [62] and provide detailed information on slope parameters [52,75]. Finally, the slope profiles created by UAV DSM are the most appropriate for 2D rockfall simulations, via RocFall software, as the extracted parameters and calculations are closer to the real measurements than those from other DSMs. Yakar et al. (2022) concluded that UAV photogrammetry is also the most preferable for 3D modeling [76]. Senkal et al. (2021) summarized that UAV measurements are as reliable as terrestrial ones [77]. Kakavas et al. (2022) accomplished a series of tests by resampling a 5 cm UAV DSM to pixel sizes with lower accuracy (1 m, 2 m, 3 m, 4 m and 5 m) and concluded that DSMs of spatial resolution lower than 1 m offer the most realistic results [78].

Another crucial parameter that is taken into account in rockfall occurrences is the vegetation cover, as it affects the path of the detached rocks. The relationship between wildfires and rockfalls has been widely studied, as wildfires cause lack of vegetation and, consequently, lead to the reduction in soil/rock cohesion [79]. DeGraff et al. (2013) highlighted that, when the wildfires that consume the vegetation of steep and rugged slopes are followed by high-intensity rain storms, destructive debris flows usually emerge [80]. Parise et al. (2012) mentioned that, over long periods, the large diameter and deep root networks of vegetation burned during the wildfires will decay [81]. Thus, instability effects may appear months or years after the fires. A review study about the influence of the lack of vegetation due to wildfires on rockfall occurrence was recently presented [82]. The existence of vegetation (grasses and shrubs) on the rockfall trajectory can affect the rocks in the same way that bedrock interacts with the rock. This is due to the increased friction exerted on the rock from these materials. Other important influences can be inserted by trees that generate large obstacles that a rock has to overcome. A tree has the potential to stop or slow a boulder. Trees with wide trunks are usually strong enough to deflect a boulder off its current trajectory. This occurs when the boulder impacts the tree trunk away from its center of mass [83]. Vegetation is used globally as a form of rockfall mitigation of the boulder. All the rockfall simulation software, such as Rocfall, assess this interaction by increasing the friction the boulder experiences in a vegetated area. In reality, the interaction between trees and boulders is not that simple. A falling or rolling rock may miss the trees altogether and, therefore, not be affected at all in its way down by this parameter; it may also experience a blow and be directed away from its current trajectory. The protective effect of mountain forests against rockfall was shown using a 3D simulation model by Stoffel et al. (2006) [84]. The energy reduction effect of vegetation was studied experimentally in detail by Dorren et al. (2005) [85]. Özdemir et al. (2021) completed an automatic extraction of trees via LIDAR point cloud [86]. In addition, an overview of the current scientific knowledge and methods concerning rockfalls and forests protecting against them was described by Dorren et al. (2007) [87]. The energy absorption of trees using a numerical single-tree model was investigated by Jonsson (2007) [88], but there are still many problems to be solved concerning evaluation of the role of vegetation against rockfalls [89]. In their study, Moos et al. (2020) used RockyFor3D for comparing the differences in forest structure as a function of tree density, tree diameter and tree species in different rockfall activity zones [90]. In a similar study, Bonneau et al. (2020) incorporated the individual tree locations and heights into rockfall runout simulations using another software named RockyFor3D [91]. Their objective was to investigate the implications of tree identification in point clouds for rockfall hazard assessments using rockfall simulations. The same software was used by Dupire et al. (2016) in order to examine the protective role of forests against rockfalls across the French Alps [92]. Jancke et al. (2009) developed a

simple 2D rockfall simulation model, named RockCop, in order to quantify the protective function of vegetation and performed nine different rockfall scenarios [93].

Thus, the existence or not and the density of vegetation is a considerable parameter for this project, as Rocfall can take this variance into account and, in our case studies, there are significant data from the site areas that can be used as input into the model. Vegetation and land cover are inserted in the modeling process of RocFall software by the tool "material editor". Therefore, each area of interest was specified according to its characteristics of vegetation and land cover in the index roughness of the slope. In the current study, the three areas can be distinguished in three categories: area with dense vegetation (Platiana), as presented in Figure 8b, area with no vegetation (Myloi), as presented in Figure 4, and area with sparse vegetation (Moira), as presented in Figure 1.

Furthermore, the vegetation density and height is a dynamic parameter that changes over time. The UAVs are the only remote sensing platform that can provide updated and close-to-the-reality data about the vegetation cover and the relief in order to feed the rockfall simulation software. In the case of Platiana rockfall, the Cadastral DSM was generated by digital orthophotos acquired on 2007–2008 after the wildfires that occurred during the summer of 2007. Figure 8a presents the slope over Platiana settlement on 2008 and there is no vegetation at all, while Figure 8b presents the same area 10 years later. The whole area is covered by dense vegetation in less than 10 years after the wildfires. All the freely available DSMs used in the current study (Table 1) are developed and released many years before the occurrence of the rockfall. Thus, any landscape or vegetation change is not applicable on those DSMs. The existence of dense vegetation influences the rockfall simulations in many ways: changing the slope gradient, increasing the friction and reducing the boulder kinetic energy or changing the boulder trajectory. At this point, it is important to underline that a DSM offers better trajectory than a DTM, as it takes vegetation into consideration and assumes that trees constitute the physical boundaries in software. Consequently, if the study area is characterized by dense vegetation that changes over time, the UAV DSM is the most dependable DSM, as it offers updated data. As Wechsler and Kroll (2006) have mentioned, researchers often use the DSM as a truth surface rather than as a model and it is their responsibility to determine whether uncertainty in the DSM will affect results from specific analyses that utilize data derived from a particular DSM [73].

6. Conclusions

In the current work, the RocFall software is selected for simulating rockfall trajectories developed in three different areas of interest (Moira, Myloi and Platiana settlements). These areas have been extensively observed since the occurrence of the rockfall events. Therefore, a plethora of in situ measurements and observations have been recorded and many geo-data sets have been collected. These data significantly contribute towards the extraction of a reliable 2D rockfall simulation, with relatively small discrepancies from the observations of the real event.

1. DSMs from UAV data with sub-decimeter spatial resolution proved to be the most accurate for a rockfall simulation in all the case studies examined in the current manuscript.
2. The UAV offers a significantly different pathway among different rocks, whereas the other DSMs have a rather stable path.
3. The DSMs can be classified into three categories according to their accuracy in rockfall simulation. In particular:
    (i) High accuracy, which corresponds to DSMs with spatial resolution less than 5 m, such as UAV DSM and DSM from the Greek Cadastral. The processing of these DSMs in RocFall software extracted results similar to in situ observations.
    (ii) Medium accuracy, which corresponds to DSMs with spatial resolutions ranging from 20 m to 30 m, such as DSM derived from the Ministry of Agriculture, ALOS AW3D30 DEM, ASTER GDEM and SRTM30 DEM. Against all these

DSMs, only DSM of the Ministry of Agriculture and ALOS AW3D30 DEM offered rockfall illustration relatively close to the real event.

(iii) Low accuracy, which corresponds to DSMs with spatial resolution of 90 m, such as SRTM90 DEM and TanDEM_X, and led to rockfall conclusions that abstain from the reality.

4. The existence of vegetation plays an important role in the simulation of the rock rolling or bouncing and a very fine DSM from UAV data can represent the present real height of the vegetation in contrast to the free available DSMs, such as SRTM DEM or ASTER DEM, that represented the planet relief and vegetation cover a few years ago.
5. The coarse resolution of SRTM 90DEM and TanDEM_X may lead to the inaccurate slope profiles and to the erroneous calculations of the barriers' influence (physical, such as roads, or technical, such as fences) on the rock bounce height and to the rock kinetic energy. Previous rockfall simulation studies based on SRTM90 or TanDEM_X DSMs should be re-evaluated.

Author Contributions: Conceptualization, M.P.K. and K.G.N.; methodology, M.P.K. and K.G.N.; software, M.P.K.; validation, K.G.N., A.K. and I.K.; investigation, K.G.N., I.K. and A.K.; data curation, K.G.N., I.K. and A.K.; writing—original draft preparation, A.K.; writing—review and editing, M.P.K., K.G.N., I.K. and A.K.; supervision, K.G.N.; project administration, K.G.N. and I.K.; funding acquisition, K.G.N. All authors have read and agreed to the published version of the manuscript.

Funding: This research was partially funded by Grant (80634) from the Research Committee of the University of Patras via "C. Caratheodori" program.

Data Availability Statement: The data presented in this study are available on request from the corresponding author.

Acknowledgments: We would like to thank the Research Committee of the University of Patras for funding via "C. Caratheodori" program.

Conflicts of Interest: The authors declare no conflict of interest.

References

1. Wyllie, D.C. *Rock Fall Engineering*; CRC Press: Boca Raton, FL, USA, 2007; 270p.
2. Calcaterra, D.; Parise, M. Weathering as a predisposing factor to slope movements: An introduction. *Geol. Soc. Lond. Eng. Geol. Spec. Publ.* **2010**, *23*, 233. [CrossRef]
3. Wyllie, D.C. Calibration of rock fall modeling parameters. *Int. J. Rock Mech. Min. Sci.* **2014**, *67*, 170–180. [CrossRef]
4. Dorren, L. A review of rockfall mechanics and modelling approaches. *Prog. Phys. Geogr.* **2003**, *27*, 69–87. [CrossRef]
5. Gutierrez, F. Hazards associated with karst. In *Geomorphological Hazards and Disaster Prevention*; Alcantara, I., Goudie, A., Eds.; Cambridge University Press: Cambridge, UK, 2010; pp. 161–175.
6. Parise, M. Rock failures in karst. In *Landslides and Engineered Slopes. From the Past to the Future, Two Volumes+ CD-ROM: Proceedings of the 10th International Symposium on Landslides and Engineered Slopes, 30 June–4 July 2008, Xi'an, China*; CRC Press: Boca Raton, FL, USA, 2008.
7. Parise, M. Hazards in karst. In Proceedings of the International Interdisciplinary Scientific Conference, Sustainability of the Karst Environment, Dinaric Karst and Other Karst Regions, Plitvice Lakes, Croatia, 23–26 September 2009.
8. Rocscience. *RocFall V.4: A Statistical Analysis Program Designed to Assist with a Risk Assessment of Slopes at Risk of Rockfalls*; Rocscience: Toronto, ON, Canada, 2004.
9. Vick, L.M. Evaluation of Field Data and 3D Modelling for Rockfall Hazard Assessment. Master's Thesis, University of Canterbury, Christchurch, New Zealand, 2015.
10. Stevens, W.D. RocFall, a Tool for Probabilistic Analysis, Design of Remedial Measures and Prediction of Rockfalls. Ph.D. Thesis, University of Toronto, Toronto, ON, Canada, 1998.
11. Palma, B.; Parise, M.; Reichenbach, P.; Guzzetti, F. Rockfall hazard assessment along a road in the Sorrento Peninsula, Campania, southern Italy. *Nat. Hazards* **2012**, *61*, 187–201. [CrossRef]
12. Sun, S.; Li, L.; Li, S.; Zhang, Q.; Hu, C. Rockfall Hazard Assessment on Wangxia Rock Mass in Wushan (Chongqing, China). *Geotech. Geol. Eng.* **2017**, *35*, 1895–1905. [CrossRef]
13. Taherynia, M.H.; Mohammadi, M.; Ajalloeian, R. Assessment of Slope Instability and Risk Analysis of Road Cut Slopes in Lashotor Pass, Iran. *J. Geol. Res.* **2014**, *2014*, 763598. [CrossRef]
14. Topal, T.; Akin, M.; Ozden, A.U. Analysis and evaluation of rockfall hazard around Afyon Castle, Turkey. In Proceedings of the 10th International Congress IAEG, Nottingham, UK, 6–10 September 2006.

15. Parise, M. Landslide hazard zonation of slopes susceptible to rock falls and topples. *Nat. Hazards Earth Syst. Sci.* **2002**, *2*, 37–49. [CrossRef]
16. Abdullah, R.A.; Fowell, R.J.; Murphy, W. Selecting shear strength models for joints-experience with modeling of complex rock slope failure in UDEC. In *ISRM International Symposium-EUROCK 2010*; International Society for Rock Mechanics and Rock Engineering: Lisbon, Portugal, 2010.
17. Andrade, P.S.; Gonçalves, G.; Quinta-Ferreira, M. Rock Fall Analysis on the City of Lubango, SW Angola. *Eng. Geol. Soc. Territ.* **2015**, *2*, 2027–2030.
18. Keskin, İ. Evaluation of rock falls in an urban area: The case of Boğaziçi (Erzincan/Turkey). *Environ. Earth Sci.* **2013**, *70*, 1619–1628. [CrossRef]
19. Caso, I.; D'Angelo, R.; Palma, B.; Parise, M.; Ruocco, A. Landslide susceptibility maps in the rock slopes of the Ventotene Island (Latium, Italy). In *Engineering Geology for Society and Territory*; Springer: Berlin/Heidelberg, Germany, 2014; pp. 941–945.
20. Ansari, M.K.; Ahmad, M.; Singh, R.; Singh, T.N. Rockfall hazard assessment at Ajanta Cave, Aurangabad, Maharashtra, India. *Arab. J. Geosci.* **2013**, *7*, 1773–1780. [CrossRef]
21. Ansari, M.K.; Ahmad, M.; Singh, R.; Singh, T.N. Rockfall assessment near saptashrungi gad temple, Nashik, Maharashtra, India. *Int. J. Disaster Risk Reduct.* **2012**, *2*, 77–83. [CrossRef]
22. E'bayat, M. Assessment of Rockfall Rollout Risk along Varying Slope Geometries Using the Rocfall and CRSP Software. Master's Thesis, Missouri University of Science and Technology, Rolla, MO, USA, 2017.
23. Guzzetti, F.; Crosta, G.; Detti, R.; Agliardi, F. STONE: A computer program for the three-dimensional simulation of rock-falls. *Comput. Geosci.* **2002**, *28*, 1079–1093. [CrossRef]
24. Hind, H. Comparison of 3D and 2D Rockfall Models: Considering Terrain Model Quality Effect on Respective Model Performances. Master's Thesis, UiT the Arctic University of Norway, Tromsø, Norway, 2018.
25. Saroglou, C.; Asteriou, P.; Zekkos, D.; Tsiambaos, G.; Clark, M.; Manousakis, J. UAV-based mapping, back analysis and trajectory modeling of a coseismic rockfall in Lefkada island, Greece. *Nat. Hazards Earth Syst. Sci.* **2018**, *18*, 321–333. [CrossRef]
26. Clayton, C.; Jackson, A.; Price, J.; Bidwell, A.; Elmo, D. Case study: Analysis of a highwall toppling failure and development of a successful mine re-entry plan using RS2, RocFall and Dan-W at a coal mine in Canada. In *Slope Stability 2020: Proceedings of the 2020 International Symposium on Slope Stability in Open Pit Mining and Civil Engineering*; Australian Centre for Geomechanics: Crawley, Australia, 2020.
27. Chun, Z.; Zhigang, T.; Sen, Y.; Shuai, Z. V shaped gully method for controlling rockfall on high-steep slopes in China. *Bull. Eng. Geol. Environ.* **2019**, *78*, 2731–2747. [CrossRef]
28. He, Y.; Nie, L.; Lv, Y.; Wang, H.; Jiang, S.; Zhao, X. The study of rockfall trajectory and kinetic energy distribution based on numerical simulations. *Nat. Hazards* **2021**, *106*, 213–233. [CrossRef]
29. Jones, C.; Higgins, J.; Richard, A. MI-66 Colorado Rockfall Simulation Program, Version 4.0. *Rockfall Simulation Program. Miscellaneous MI-66. Denver, CO: Colorado Geological Survey, Division of Minerals and Geology, Department of Natural Resources, March 2000*. Available online: https://coloradogeologicalsurvey.org/publications/colorado-rockfall-simulation-program/ (accessed on 8 February 2023).
30. Yilmaz, M.; Uysal, M. Comparing uniform and random data reduction methods for DTM accuracy. *Int. J. Eng. Geosci.* **2017**, *2*, 9–16. [CrossRef]
31. Fanos, A.M.; Pradhan, B. Laser Scanning Systems and Techniques in Rockfall Source Identification and Risk Assessment: A Critical Review. *Earth Syst. Environ.* **2018**, *2*, 163–182. [CrossRef]
32. Depountis, N.; Nikolakopoulos, K.; Kavoura, K.; Sabatakakis, N. Description of a GIS-based rockfall hazard assessment methodology and its application in mountainous sites. *Bull. Eng. Geol. Environ.* **2019**, *79*, 645–658. [CrossRef]
33. Othman, A.; Shaaban, F.; Abotalib, A.Z.; El-Saoud, W.A.; Gabr, S.S.; Habeebullah, T.; Hegazy, D. Hazard assessment of rockfalls in mountainous urban areas, western Saudi Arabia. *Arab. J. Sci. Eng.* **2020**, *46*, 5717–5731. [CrossRef]
34. Hatzfeld, D.; Pedotti, G.; Hatzidimitriou, P.; Makropoulos, K. The strain pattern in the western Hellenic arc deduced from amicroearthquake survey. *Geophys. J. Int.* **1990**, *101*, 181–202. [CrossRef]
35. Kokkalas, S.; Xypolias, P.; Koukouvelas, I.; Doutsos, T. Postcollisional contractional and extensional deformation in the Aegean region. In *Postcollisional Tectonics and Magmatism in the Mediterranean Region and Asia*; Geological Society of America: Boulder, CO, USA, 2006; pp. 97–123.
36. Koukis, G.; Sabatakakis, N.; Nikolau, N.; Loupasakis, C. Landslide Hazard Zonation in Greece. In *Landslides: Risk Analysis and Sustainable Disaster Management*; Springer Science & Business Media: Berlin/Heidelberg, Germany, 2005; pp. 291–296.
37. Sabatakakis, N.; Koukis, G.; Vassiliades, E.; Lainas, S. Landslide susceptibility zonation in Greece. *Nat. Hazards* **2012**, *65*, 523–543. [CrossRef]
38. Kyriou, A.; Nikolakopoulos, K.; Koukouvelas, I.; Lampropoulou, P. Repeated UAV campaigns, GNSS measurements, GIS, and petrographic analyses for landslide mapping and monitoring. *Minerals* **2021**, *11*, 300. [CrossRef]
39. Kakavas, M.; Nikolakopoulos, K. Rock-fall simulation and validation with in situ data: The case of Moira settlement in Western Greece. In *Earth Resources and Environmental Remote Sensing/GIS Applications XII*; SPIE: Madrid, Spain, 2021.
40. Depountis, N.; Lainas, S.; Pyrgakis, D.; Sabatakakis, N.; Koukis, G. Engineering geological and geotechnical investigation of landslide events in wildfire affected areas of Ilia Prefecture, Western Greece. *Bull. Geol. Soc. Greece* **2010**, *43*, 1138–1148. [CrossRef]

41. Vagenas, N. Rockfall Simulation by Analytical Methods. Correlation of Rockfall Energy Dissipation Parameters and Rock Mass Characteristics. Ph.D. Thesis, University of Patras, Patras, Greece, 2020.
42. Kyriou, A.; Kakavas, M.; Nikolakopoulos, K.; Koukouvelas, I.; Stefanopoulos, P.; Zygouri, V.; Tsigalidas, D. Landslide mapping and volume estimation using UAV-based point clouds, GIS and geophysical techniques. In *Earth Resources and Environmental Remote Sensing/GIS Applications XI*; SPIE: Edinburg, UK, 2020.
43. Sabatakakis, N.; Depountis, N.; Vagenas, N. Evaluation of Rockfall Restitution Coefficients. *Eng. Geol. Soc. Territ.* **2015**, *2*, 2023–2026.
44. Yilmaz, I.; Yildirim, M.; Keskin, I. A method for mapping the spatial distribution of RockFall computer program analyses results using ArcGIS software. *Bull. Eng. Geol. Environ.* **2008**, *67*, 547–554. [CrossRef]
45. Rocscience. RocFall software—For risk analysis of falling rocks on steep slopes. In *Rocscience User's Guide*; Rocscience: Toronto, ON, Canada, 2002.
46. Verma, A.K.; Sardana, S.; Sharma, P.; Dinpuia, L.; Singh, T.N. Investigation of rockfall-prone road cut slope near Lengpui Airport, Mizoram, India. *J. Rock Mech. Geotech. Eng.* **2018**, *11*, 146–158. [CrossRef]
47. Souisa, M.; Hendrajaya, L.; Handayani, G. Study on Estimates of Travel Distance, Velocity and Potential Volume of Amahusu Sliding Plane using Energy Conservation Approach in Conjunction with Geoelectric Survey. *J. Math. Fundam. Sci.* **2018**, *50*, 166–181. [CrossRef]
48. Papathanassiou, G.; Marinos, V.; Vogiatzis, D.; Valkaniotis, S. A rock fall analysis study in Parnassos area, Central Greece. In *Landslide Science and Practice*; Springer: Berlin/Heidelberg, Germany, 2013; pp. 67–72.
49. Budetta, P. Assessment of rockfall risk along roads. *Nat. Hazards Earth Syst. Sci.* **2004**, *4*, 71–81. [CrossRef]
50. Katz, O.; Reichenbach, P.; Guzzetti, F. Rock fall hazard along the railway corridor to Jerusalem, Israel, in the Soreq and Refaim valleys. *Nat. Hazards* **2011**, *56*, 649–665. [CrossRef]
51. Budetta, P.; De Luca, C.; Nappi, M. Quantitative rockfall risk assessment for an important road by means of the rockfall risk management (RO. MA.) method. *Bull. Eng. Geol. Environ.* **2016**, *75*, 1377–1397. [CrossRef]
52. Kakavas, M.; Nikolakopoulos, K. Digital Elevation Models of Rockfalls and Landslides: A Review and Meta-Analysis. *Geosciences* **2021**, *11*, 256. [CrossRef]
53. Kawabata, D.; Bandibas, J. Landslide susceptibility mapping using geological data, a DEM from ASTER images and an Artificial Neural Network (ANN). *Geomorphology* **2009**, *113*, 97–109. [CrossRef]
54. Oh, H.J.; Park, N.W.; Lee, S.S.; Lee, S. Extraction of landslide-related factors from ASTER imagery and its application to landslide susceptibility mapping. *Int. J. Remote Sens.* **2012**, *33*, 3211–3231. [CrossRef]
55. Fuchs, M.; Torizin, J.; Kühn, F. The effect of DEM resolution on the computation of the factor of safety using an infinite slope model. *Geomorphology* **2014**, *224*, 16–26. [CrossRef]
56. Mahalingam, R.; Olsen, M.J. Evaluation of the influence of source and spatial resolution of DEMs on derivative products used in landslide mapping. Geomat. *Nat. Hazards Risk* **2015**, *7*, 1835–1855. [CrossRef]
57. Rasyid, A.R.; Bhandary, N.P.; Yatabe, R. Performance of frequency ratio and logistic regression model in creating GIS based landslides susceptibility map at Lompobattang Mountain, Indonesia. *Geoenviron. Dis.* **2016**, *3*, 19. [CrossRef]
58. Wang, Q.; Li, W.; Wu, Y.; Pei, Y.; Xie, P. Application of statistical index and index of entropy methods to landslide susceptibility assessment in Gongliu (Xinjiang, China). *Environ. Earth Sci.* **2016**, *75*, 599. [CrossRef]
59. Pradhan, B.; Sameen, M.I. Effects of the Spatial Resolution of Digital Elevation Models and Their Products on Landslide Susceptibility Mapping. In *Laser Scanning Applications in Landslide Assessment*; Springer: Cham, Switzerland, 2017; pp. 133–150.
60. Juliev, M.; Mergili, M.; Mondal, I.; Nurtaev, B.; Pulatov, A.; Hübl, J. Comparative analysis of statistical methods for landslide susceptibility mapping in the Bostanlik District, Uzbekistan. *Sci. Total Environ.* **2018**, *653*, 801–814. [CrossRef]
61. McLean, A. Landslide Risk Assessment Using Digital Elevation Models. Master's Thesis, Dalhousie University, Halifax, NS, Canada, 2011.
62. Fenton, G.A.; McLean, A.; Nadim, F.; Griffiths, D.V. Landslide hazard assessment using digital elevation models. *Can. Geotech. J.* **2013**, *50*, 620–631. [CrossRef]
63. Calvello, M.; Cascini, L.; Mastroianni, S. Landslide zoning over large areas from a sample inventory by means of scale-dependent terrain units. *Geomorphology* **2013**, *182*, 33–48. [CrossRef]
64. Huang, Y.; Yu, M.; Xu, Q.; Sawada, K.; Moriguchi, S.; Yashima, A.; Liu, C.; Xue, L. InSAR-derived digital elevation models for terrain change analysis of earthquake-triggered flow-like landslides based on ALOS/PALSAR imagery. *Environ. Earth Sci.* **2014**, *73*, 7661–7668. [CrossRef]
65. Gorum, T.; Fan, X.; van Westen, C.J.; Huang, R.Q.; Xu, Q.; Tang, C.; Wang, G. Distribution pattern of earthquake-induced landslides triggered by the 12 May 2008 Wenchuan earthquake. *Geomorphology* **2011**, *133*, 152–167. [CrossRef]
66. Chen, Q.; Liu, X.; Liu, C.; Ji, R. Impact Analysis of Different Spatial Resolution DEM on Object-Oriented Landslide Extraction from High Resolution Remote Sensing Images. In Proceedings of the 2013 Ninth International Conference on Natural Computation (ICNC), Shenyang, China, 23–25 July 2013; IEEE: Piscataway, NJ, USA, 2013; pp. 940–945.
67. Žabota, B.; Repe, B.; Kobal, M. Influence of digital elevation model resolution on rockfall modelling. *Geomorphology* **2019**, *328*, 183–195. [CrossRef]
68. Lee, S.; Choi, J.; Woo, I. The effect of spatial resolution on the accuracy of landslide susceptibility mapping: A case study in Boun, Korea. *Geosci. J.* **2004**, *8*, 51–60. [CrossRef]

69. Claessens, L.; Heuvelink, G.B.M.; Schoorl, J.M.; Veldkamp, A. DEM resolution effects on shallow landslide hazard and soilredistribution modelling. *Earth Surf. Proc. Landf.* **2005**, *30*, 461–477. [CrossRef]
70. Kakavas, M.; Kyriou, A.; Nikolakopoulos, K.G. Assessment of Freely Available DSMs for Landslide-Rockfall Studies. In *Earth Resources and Environmental Remote Sensing/GIS Applications XI*; SPIE: Edinburg, UK, 2020; pp. 149–156.
71. Ravanel, L.; Allignol, F.; Deline, P.; Gruber, S.; Ravello, M. Rock falls in the Mont Blanc Massif in 2007 and 2008. *Landslides* **2010**, *7*, 493–501. [CrossRef]
72. Wechsler, S.P. Uncertainties associated with digital elevation models for hydrologic applications: A review. *Hydrol. Earth Syst. Sci.* **2007**, *11*, 1481–1500. [CrossRef]
73. Wechsler, S.P.; Kroll, C.N. Quantifying DEM uncertainty and its effect on topographic parameters. *Photogramm. Eng. Remote Sens.* **2006**, *72*, 1081–1090. [CrossRef]
74. Loye, A.; Jaboyedoff, M.; Pedrazzini, A. Identification of potential rockfall source areas at a regional scale using a DEM-based geomorphometric analysis. *Nat. Hazards Earth Syst. Sci.* **2009**, *9*, 1643–1653. [CrossRef]
75. Baillifard, F.; Jaboyedoff, M.; Sartori, M. Rockfall hazard mapping along a mountainous road in Switzerland using a GIS based parameter rating approach. *Nat. Hazards Earth Syst. Sci.* **2003**, *3*, 435–442. [CrossRef]
76. Yakar, M.; Ulvi, A.; Yiğit, A.Y.; Alptekin, A. Discontinuity set extraction from 3D point clouds obtained by UAV Photogrammetry in a rockfall site. *Surv. Rev.* **2022**, 1–13. [CrossRef]
77. Senkal, E.; Kaplan, G.; Avdan, U. Accuracy assessment of digital surface models from unmanned aerial vehicles' imagery on archaeological sites. *Int. J. Eng. Geosci.* **2021**, *6*, 81–89. [CrossRef]
78. Kakavas, M.P.; Nikolakopoulos, K.G. The influence of DSM on rock-fall simulation: A case study from western Greece. In *Earth Resources and Environmental Remote Sensing/GIS Applications XIII*; SPIE: Berlin, Germany, 2022; pp. 272–284.
79. Cannon, S.H.; Gartner, J.E.; Rupert, M.G.; Michael, J.A.; Rea, A.H.; Parrett, C. Predicting the probability and volume of postwildfire debris flows in the intermountain western United States. *Geol. Soc. Am. Bull.* **2009**, *122*, 127–144. [CrossRef]
80. DeGraff, J.V.; Cannon, S.H.; Parise, M. Limiting the Immediate and Subsequent Hazards Associated with Wildfires. In *Landslide Science and Practice: Volume 4: Global Environmental Change*; Springer Science & Business Media: Berlin/Heidelberg, Germany, 2013; pp. 199–209.
81. Parise, M.; Cannon, S.H. Wildfire impacts on the processes that generate debris flows in burned watersheds. *Nat. Hazards* **2012**, *61*, 217–227. [CrossRef]
82. Sarro, R.; Pérez-Rey, I.; Tomás, R.; Alejano, L.R.; Hernández-Gutiérrez, L.E.; Mateos, R.M. Effects of Wildfire on Rockfall Occurrence: A Review through Actual Cases in Spain. *Appl. Sci.* **2021**, *11*, 2545. [CrossRef]
83. Bourrier, F.; Dorren, L.; Nicot, F.; Berger, F.; Darve, F. Toward objective rockfall trajectory simulation using a stochastic impact model. *Geomorphology* **2009**, *110*, 68–79. [CrossRef]
84. Stoffel, M.; Wehrli, A.; Kuhne, R.; Dorren, L.K.A.; Perret, S.; Kienholz, H. Assessing the protective effect of mountain forests against rockfall using a 3D simulation model. *For. Ecol. Manag.* **2006**, *225*, 113–122. [CrossRef]
85. Dorren, L.; Berger, F. Stem breakage of trees and energy dissipation during rockfall impacts. *Tree Physiol.* **2005**, *26*, 63–71. [CrossRef]
86. Özdemir, S.; Akbulut, Z.; Karsli, F.; Hayrettin, A.C.A.R. Automatic extraction of trees by using multiple return properties of the lidar point cloud. *Int. J. Eng. Geosci.* **2021**, *6*, 20–26. [CrossRef]
87. Dorren, L.; Berger, F.; Jonsson, M.; Krautblatter, M.; Molk, M.; Stoffel, M.; Wehrli, A. State of the art in rockfall-forest interactions. *Schweiz. Z. Forstwes.* **2007**, *158*, 128–141. [CrossRef]
88. Jonsson, M. Energy Absorption of Trees in a Rockfall Protection Forest. Ph.D. Thesis, ETH Zurich, Zürich, Switzerland, 2007.
89. Masuya, H.; Amanuma, K.; Nishikawa, Y.; Tsuji, T. Basic rockfall simulation with consideration of vegetation and application to protection measure. *Nat. Hazards Earth Syst. Sci.* **2009**, *9*, 1835–1843. [CrossRef]
90. Moos, C.; Khelidj, N.; Guisan, A.; Lischke, H.; Randin, C.F. A quantitative assessment of rockfall influence on forest structure in the Swiss Alps. *Eur. J. For. Res.* **2021**, *140*, 91–104. [CrossRef]
91. Bonneau, D.A.; DiFrancesco, P.M.; Hutchinson, D.J. A method for vegetation extraction in mountainous terrain for rockfall simulation. *Remote Sens. Environ.* **2020**, *251*, 112098. [CrossRef]
92. Dupire, S.; Bourrier, F.; Monnet, J.M.; Bigot, S.; Borgniet, L.; Berger, F.; Curt, T. The protective effect of forests against rockfalls across the French Alps: Influence of forest diversity. *For. Ecol. Manag.* **2016**, *382*, 269–279. [CrossRef]
93. Jancke, O.; Dorren, L.K.; Berger, F.; Fuhr, M.; Köhl, M. Implications of coppice stand characteristics on the rockfall protection function. *For. Ecol. Manag.* **2009**, *259*, 124–131. [CrossRef]